

1 **An FGF-driven feed-forward circuit for spatiotemporal patterning of the
2 cardiopharyngeal mesoderm in a simple chordate**

3

4 Florian Razy-Krajka, Basile Gravez and Lionel Christiaen*

5

6 Center for Developmental Genetics, Department of Biology, College of Arts and Science,

7 New York University, New York, NY, USA

8

9 * author for correspondence: email: lc121@nyu.edu, twitter: @lionlchristiaen, phone: +1

10 212 992 8695

11

12 **Abstract**

13 In embryos, pluripotent stem cells and multipotent progenitors must divide and produce
14 distinct progeny to express their full developmental potential. In vertebrates, mounting
15 evidence point to the existence of multipotent cardiopharyngeal progenitors that
16 produce second-heart-field-derived cardiomyocytes, and branchiomeric skeletal head
17 muscles. However, the cellular and molecular mechanisms underlying these early fate
18 choices remain largely elusive. The tunicate *Ciona* has emerged as an attractive model to
19 study early cardiopharyngeal development at high spatial and temporal resolution:
20 through two asymmetric and oriented cell divisions, defined multipotent
21 cardiopharyngeal progenitors produce distinct first and second heart precursors, and
22 pharyngeal muscle (aka atrial siphon muscle, ASM) precursors. Here, we demonstrate
23 that differential FGF/MAPK signaling distinguishes between MAPK-negative heart
24 precursors, and MAPK-positive multipotent progenitors and ASM precursors. We
25 characterize an FGF/MAPK-driven feed-forward circuit that promotes the successive
26 activations of essential cardiopharyngeal determinants, *Tbx1/10* and *Ebf*. Finally, we
27 show that coupling FGF/MAPK restriction and cardiopharyngeal network deployment
28 with cell divisions permits the emergence of diverse cell types from common multipotent
29 progenitors.

30 **Introduction**

31 In the past few years, studies guided by developmental genetics knowledge
32 progressed towards driving mammalian stem cells into forming pure cultures of selected
33 cell types *in vitro* (e.g. (Kattman et al., 2011; Mazzoni et al., 2011; Peljto and Wichterle,
34 2011). By contrast, in their embryonic context, pluripotent cells generate diverse cell
35 types in defined proportions. This simple observation implies that pluripotent stem cells
36 and multipotent embryonic progenitors must divide before individual cells among their
37 progeny adopt distinct fates, as a result of differential exposure to inducing signals
38 and/or inheritance of cell autonomous determinants.

39 Subsets of the heart and head/neck myocytes recently emerged as related derivatives
40 of multipotent progenitors located in the mesodermal cardiopharyngeal field (Diogo et
41 al., 2015; Tzahor, 2009; Tzahor and Evans, 2011). Specifically, early lineage tracing,
42 transplantations and controlled explant culture experiments demonstrated that the
43 anterior splanchnic/pharyngeal mesoderm of amniote embryos can produce either
44 skeletal muscles or heart tissue, depending upon exposure to growth factors and
45 signaling molecules (Nathan et al., 2008; Tirosh-Finkel et al., 2006; Tzahor et al., 2003;
46 Tzahor and Lassar, 2001). Clonal analyses in the mouse further revealed the existence of
47 common *Mesp1*-expressing progenitors for subsets of the second heart field-derived
48 cardiomyocytes and branchiomeric facial, jaw, neck and even esophageal muscles
49 (Gopalakrishnan et al., 2015; Lescroart et al., 2014; Lescroart et al., 2015; Lescroart et
50 al., 2010; Lescroart et al., 2012). *In vitro* studies using pluripotent stem cells indicated
51 that controlled *Mesp1* expression can drive mesodermal progenitors towards cardiac
52 and/or skeletal muscle fates (Bondué et al., 2008; Chan et al., 2016; Chan et al., 2013).
53 Genetic labeling and functional studies showed that proper development of the
54 pharyngeal apparatus and second heart field derivatives require shared inputs from
55 *Tbx1*, *Nkx2-5* and *Islet1* transcription factors (e.g. (Cai et al., 2003; George et al., 2015;

56 Jerome and Papaioannou, 2001; Kelly et al., 2004; Merscher et al., 2001; Mosimann et
57 al., 2015; Nevis et al., 2013; Prall et al., 2007; Tzahor and Evans, 2011; Vitelli et al.,
58 2002a; Watanabe et al., 2012; Witzel et al., 2017; Yagi et al., 2003; Zhang et al., 2006)).
59 Taken together, a growing body of evidence point to the existence of a mesodermal field
60 of multipotent progenitors capable of producing either SHF-derived cardiomyocytes or
61 branchiomeric skeletal muscles in early amniote embryos (Diogo et al., 2015; Mandal et
62 al., 2017). However, the mechanisms that distinguish fate-restricted heart and head
63 muscle precursors remain largely elusive.

64 The tunicate *Ciona*, which is among the closest living relatives to the vertebrates
65 (Delsuc et al., 2006; Putnam et al., 2008), has emerged as a simple chordate model to
66 characterize multipotent cardiopharyngeal progenitors and the mechanisms that initiate
67 heart vs. pharyngeal muscle fate choices (Kaplan et al., 2015; Razy-Krajka et al., 2014;
68 Stolfi et al., 2010; Tolkin and Christiaen, 2016; Wang et al., 2013). *Ciona* tailbud
69 embryos possess two multipotent cardiopharyngeal progenitors on either side. Like their
70 vertebrate counterparts, these cells emerge from *Mesp*+ progenitors towards the end of
71 gastrulation; they are induced by FGF/MAPK signaling and have been termed *trunk*
72 *ventral cells* (aka TVCs; (Christiaen et al., 2008; Davidson and Levine, 2003; Davidson
73 et al., 2006; Davidson et al., 2005; Satou et al., 2004; Stolfi et al., 2010)). TVCs activate
74 conserved cardiac markers, including *Hand*, *Gata4/5/6* and *Nk4/Nkx2-5*, and migrate
75 as bilateral polarized pairs of cells, until the left and right pairs meet at the ventral
76 midline and begin to divide asymmetrically along the mediolateral axis (Figure 1A;
77 (Christiaen et al., 2008; Davidson et al., 2005; Satou et al., 2004; Stolfi et al., 2010)).
78 The first oriented asymmetric divisions produce small median first heart precursors
79 (FHPs), and large lateral second trunk ventral cells (STVCs), which specifically activate
80 *Tbx1/10* expression (Davidson et al., 2005; Stolfi et al., 2010; Wang et al., 2013). STVCs
81 later divide again to produce small median second heart precursors (SHPs), and large

82 lateral atrial siphon muscle founder cells (ASMFs), which activate *Ebf* (aka *COE*; (Razy-
83 Krajka et al., 2014; Stolfi et al., 2010; Stolfi et al., 2014c)). The transcription factors
84 Hand-related (Hand-r)/Notrlc, which is expressed in the TVCs and maintained in the
85 STVCs and ASMFs after each division, and *Tbx1/10* are required for *Ebf* activation in the
86 ASMFs, whereas *Nk4/Nkx2-5* represses *Tbx1/10* and *Ebf* expression in the second heart
87 precursors (SHPs)(Razy-Krajka et al., 2014; Tolkin and Christiaen, 2016; Wang et al.,
88 2013). Conversely, *Tbx1/10* and *Ebf* inhibit cardiac markers, and likely determinants,
89 such as *Gata4/5/6* and *Hand* (Razy-Krajka et al., 2014; Stolfi et al., 2010; Stolfi et al.,
90 2014a; Wang et al., 2013). These regulatory cross-antagonisms presumably underlie the
91 transition from transcriptionally primed multipotent progenitors to separate fate-
92 restricted precursors, by limiting the deployment of the heart- and pharyngeal-muscle-
93 specific programs to their corresponding specific precursors (Kaplan et al., 2015).

94 Here, we identify regulatory mechanisms ensuring the emergence of diverse fate-
95 restricted precursors from multipotent progenitors. We show that differential
96 FGF/MAPK signaling, feed-forward regulatory mechanisms and coupling with the cell
97 cycle control the spatially restricted activation of *Tbx1/10* and *Ebf*, successively, thus
98 permitting the emergence of both first and second heart precursors, and
99 ASM/pharyngeal muscle precursors from common multipotent progenitors.

100

101 **Results**

102 **MAPK signaling is active in the multipotent cardiopharyngeal progenitors
103 and progressively restricted to the pharyngeal muscle precursors.**

104 During the earliest stages of cardiopharyngeal development in ascidians, multipotent
105 progenitors co-express early regulators of both the heart and ASM programs, a
106 phenomenon referred to as multilineage transcriptional priming, (Razy-Krajka et al.,
107 2014; Stolfi et al., 2014b). Subsequent regulatory cross-antagonisms lead to the
108 segregation of these distinct cardiopharyngeal programs to their corresponding fate-
109 restricted progenitors (Stolfi et al., 2010; Wang et al., 2013); reviewed in (Kaplan et al.,
110 2015)). ASM-specific expression of *Ebf* is necessary and sufficient to terminate the heart
111 program and impose a pharyngeal muscle fate (Razy-Krajka et al., 2014; Stolfi et al.,
112 2010). Antagonistic *Tbx1/10* and *Nk4* activities determine ASM-specific *Ebf* activation
113 (Wang et al., 2013); however, the symmetry-breaking events leading to cardiopharyngeal
114 mesoderm patterning and ASM-specific expression of *Ebf* remain unknown. In
115 particular, we surmised that differential signaling inputs determine the stereotyped
116 spatio-temporal patterning of early cardiopharyngeal progenitors.

117 The *Ciona* homologs of specific FGF/MAPK pathway components, including *FGF*
118 *receptor substrate 2/3* (*Frs2/3*; (Gotoh et al., 2004)), *Ets.b*, and *Fgf4/5/6*, are
119 preferentially expressed in the TVCs, in the STVCs and in the ASMFs as cells transition
120 from a multipotent progenitor state to distinct heart vs. ASM fate-restricted precursors
121 (Razy-Krajka et al., 2014). This patterned expression of MAPK effector genes prompted
122 us to evaluate a role for FGF/MAPK pathway in cardiopharyngeal fate decisions.

123 We first used an antibody specific to the dual phosphorylated form of Extracellular
124 Regulated Kinase (dpERK) to monitor Mitogen Activated Protein Kinase (MAPK)
125 activity in the cardiopharyngeal mesoderm. We detected dpERK staining in the newly

126 born TVCs, marked by the B7.5-lineage-specific *Mesp>H2B::mCherry* transgene, as
127 previously observed (Davidson et al, 2006). We also detected weaker but persistent
128 dpERK staining in the TVCs during migration (Figs. 1 and S1). Following the first and
129 second asymmetric divisions of the TVCs and STVCs, dpERK staining was successively
130 restricted to the more lateral STVCs and ASMFs, respectively (Figures 1A, B; S1).

131

132 **The canonical FGF/Ras/MEK/ERK pathway is necessary and sufficient to**
133 **promote pharyngeal muscle specification in the cardiopharyngeal lineage.**

134 This exclusion of MAPK activity from the medial first and second heart precursors
135 opened the possibility that differential ERK activity is required for proper STVC and
136 ASMF vs. heart precursors fate decisions. In *Ciona*, signaling through the sole FGF
137 receptor (FGFR) governs ERK activity in several developmental processes, including
138 neural induction (Bertrand et al., 2003; Hudson et al., 2003) and central nervous system
139 patterning (Haupaix et al., 2014; Racioppi et al., 2014; Stolfi et al., 2011; Wagner et al.,
140 2014), early endomesoderm and notochord fate specification (Imai et al., 2002; Picco et
141 al., 2007; Shi and Levine, 2008; Shi et al., 2009; Yasuo and Hudson, 2007). Notably,
142 FGF/MAPK signaling is active in the only *Mesp+* cardiogenic B7.5 blastomeres (Imai et
143 al., 2006; Shi and Levine, 2008), where targeted misexpression of a dominant negative
144 form of FGFR (dnFGFR) using a B7.5-lineage-specific *Mesp* driver blocks TVC induction
145 (Davidson et al., 2006). We used a TVC-specific *FoxF* enhancer (*FoxF(TVC):bpFOG-*
146 *1>dnFGFR::mCherry*, hereafter called *FoxF>dnFGFR*; (Beh et al., 2007)), to bypass
147 early effects and achieve later misexpression of dnFGFR in the TVCs and their progeny.
148 *FoxF>dnFGFR* prevented neither TVC migration nor asymmetric divisions, but it
149 abolished the expression of both *Tbx1/10* in the STVCs and *Ebf* in the ASMFs (Figure
150 1C). This data indicate that FGF/MAPK signaling is required in the cardiopharyngeal

151 progenitors and/or their progeny for ASM fate specification, beyond the initial TVC
152 induction.

153 Upon FGF/MAPK-dependent induction, the TVCs express *Hand-related/Hand-r*
154 (renamed after *Notrlc/Hand-like*; (Christiaen et al., 2008; Davidson and Levine, 2003;
155 Davidson et al., 2006; Satou et al., 2004; Stolfi et al., 2014c; Woznica et al., 2012)),
156 which encodes a basic helix-loop-helix (bHLH) transcription factor necessary for *Ebf*
157 expression in the ASMFs (Razy-Krajka et al, 2014). Moreover, the *Hand-r* TVC enhancer
158 contains putative Ets1/2 binding sites, which are necessary for reporter gene expression,
159 and presumably mediate the transcriptional inputs of FGF/MAPK (Woznica et al., 2012).
160 Since *Hand-r* and *FoxF* expressions start at approximately the same time in newborn
161 TVCs, we used *FoxF>dnFGFR* to test whether the maintenance of *Hand-r* expression in
162 migratory TVCs requires prolonged FGF/MAPK inputs after initial TVC induction.
163 *FoxF>dnFGFR* inhibited *Hand-r* expression in late TVCs (Figure 1C), indicating that
164 sustained *Hand-r* expression requires continuous FGF/MAPK signaling.

165 To test whether the spatial restriction of MAPK activity explains the patterned
166 expressions of *Hand-r*, *Tbx1/10* and *Ebf* following asymmetric cell divisions, we used
167 gain-of-function perturbations to force FGF/MAPK activity throughout the
168 cardiopharyngeal mesoderm and assayed gene expression (Figure 2). We focused on the
169 canonical FGF/MAPK pathway where signal transduction involves Ras, Raf, MEK and
170 ERK downstream of FGFR and upstream of transcriptional effectors (Lemmon and
171 Schlessinger, 2010). We first used M-Ras^{G22V}, a defined constitutively active form of M-
172 Ras, which mediates FGF signaling in *Ciona*, where other classical *Ras* genes are missing
173 (Keduka et al., 2009). To assay the transcriptional consequences of forced M-Ras activity
174 in the cardiopharyngeal lineage, we first focus on *Htr7* and *Tbx1/10* expression following
175 the first asymmetric TVC division in 15 hours post-fertilization (hpf) embryos. *Htr7*
176 encodes a *trans*-membrane G-protein coupled receptor and, like *Hand-r*, its expression

177 and maintenance in the TVCs require MAPK activity (Figure S2; (Razy-Krajka et al.,
178 2014)), and become restricted to the lateral STVC following asymmetric division.
179 However, *Htr7* mRNAs appear to be cleared more rapidly from the FHPs, making the
180 patterned expression easier to analyze than that of *Hand-r* (Figures 2 and 3D; (Razy-
181 Krajka et al., 2014)). Importantly, misexpression of M-Ras^{G22V} using the TVC-specific
182 *FoxF* enhancer did not alter the cell division patterns, allowing us to identify large lateral
183 STVCs and small median FHPs. Compared to control embryos overexpressing wild-type
184 M-Ras (M-Ras^{WT}), TVC-specific gain of M-Ras function caused both persistent *Htr7*
185 expression and ectopic activation of *Tbx1/10* in the first heart precursors following
186 asymmetric divisions. Similarly, *FoxF>M-Ras^{G22V}*-expressing 18hpf larvae displayed
187 ectopic *Ebf* activation throughout the cardiopharyngeal mesoderm (Figure 2B, C). These
188 results indicated that forced M-Ras activation throughout the cardiopharyngeal lineage
189 is sufficient to ectopically activate STVC and ASM markers. This is consistent with the
190 idea that spatially defined signaling upstream of M-Ras restricts MAPK activity, thus
191 localizing STVC- and ASM-specific gene activities.

192 To further probe the signal transduction pathway, we engineered a constitutively
193 active version of the *Ciona* Mek1/2 protein by introducing phosphomimetic mutations of
194 two conserved serine residues in the catalytic domain, as previously shown for the
195 mammalian homolog (Cowley et al., 1994; Mansour et al., 1994). Early misexpression of
196 this *Mek^{S220E,S216D}* construct in the B7.5 blastomeres using a *Mesp* enhancer caused
197 ectopic TVC induction, mimicking the effects of published gain of *Ets1/2* function
198 (Figure S3; (Davidson et al., 2006)). Mirroring the effects of M-Ras^{G22V} gain-of-function
199 experiments, TVC-specific misexpression of *Mek^{S220E,S216D}* using the *FoxF* enhancer also
200 caused ectopic expression of *Htr7* and *Tbx1/10*, and *Ebf* in 15 and 18hpf larvae,
201 respectively (Figure 2B, C). Taken together, these results indicate that activity of the
202 canonical FGF-Ras-MEK-ERK pathway is progressively restricted to the STVC and

203 ASMF, and is both necessary and sufficient to promote STVC- and ASMF-specific gene
204 expressions.

205

206 **Continuous FGF/MAPK activity is required for the successive activations of**
207 ***Tbx1/10* and *Ebf*.**

208 FGF/MAPK signaling is sufficient and necessary to maintain *Hand-r* expression in
209 late TVCs (Figure 1), and *Hand-r* is necessary for *Ebf* expression in the ASMF (Razy-
210 Krajka et al., 2014). Therefore, it is possible that later FGF/MAPK signaling is
211 dispensable for *Tbx1/10* and *Ebf* activation and ASM specification, as long as STVC and
212 ASMF cells inherit sustained levels of *Hand-r* mRNAs and/or proteins. To disentangle
213 late from early requirements of FGF/MAPK signaling for TVC progeny specification, we
214 incubated embryos at different stages with the MEK/Mapkk inhibitor U0126, which
215 abolishes dual ERK phosphorylation and the initial MAPK-dependent TVC induction in
216 *Ciona* embryos (Figure S1; (Davidson et al., 2006; Hudson et al., 2003)). MEK inhibition
217 during TVC migration (i.e. between 9.5 and 12.5 hpf, Figure 3A) blocked the expression
218 of *Hand-r* and *Htr7* in late TVCs (Figure 3B, E). Similarly, U0126 treatments in late
219 TVCs, and through the first asymmetric division (i.e. between 12 and 15 hpf, Figure 3A)
220 blocked both the maintenance of *Hand-r* and *Htr7*, and the activation of *Tbx1/10* in the
221 STVCs (Figure 3C, D, F, G). Finally, MEK inhibition in late STVCs and through
222 asymmetric divisions (i.e. between 15 and 18 hpf) blocked the ASMF-specific expression
223 of *Ebf* (Figure 3H). These results indicate that continuous MEK activity is required
224 throughout cardiopharyngeal development to successively activate TVC-, STVC-, and
225 ASMF-expressed genes.

226 Since *Ebf* expression is maintained for several days in the ASMF derivatives as they
227 differentiate into body wall and siphon muscles (Razy-Krajka et al., 2014), we tested
228 whether continued MEK activity is also required for the maintenance of *Ebf* expression

229 past its initial onset and cells' commitment to an ASM fate. Using both regular and
230 intron-specific antisense probes, which specifically detect nascent transcripts (Wang et
231 al., 2013), we showed that later MEK inhibition (i.e. U0126 incubation between 17 and
232 20 hpf) did not block the maintenance of *Ebf* transcription in the ASMPs (Figure 3I, J).
233 This indicates that sustained MEK activity is required until the onset of *Ebf* expression,
234 but not beyond, the maintenance of *Ebf* expression during ASM development is
235 independent of MAPK.

236

237 Since U0126 treatments affect the whole embryo, we sought to further confirm the
238 later roles for FGF/MAPK signaling specifically in the cardiopharyngeal mesoderm. To
239 this aim, we used an STVC-specific enhancer from the *Tbx1/10* locus (termed *T12*; Figure
240 3K, L; (Tolkin and Christiaen, 2016); Racioppi et al., in preparation) to drive expression
241 of either dnFGFR or the constitutively active M-Ras^{G22V} starting at ~14hpf, and assayed
242 *Ebf* expression at 18hpf (Figure 3K, L). These perturbations minimally affected the cell
243 division patterns, such that cells corresponding to FHP, SHP and ASMF could be
244 identified by their position relative to the midline (Figure 3K). M-Ras^{G22V} misexpression
245 caused conspicuous ectopic *Ebf* expression in the SHPs, whereas dnFGFR-mediated
246 inhibition of MAPK activity blocked *Ebf* activation in the lateral ASMFs. These results
247 support the notion that localized FGF/MAPK activity is necessary and sufficient for
248 ASMF-specific expression of *Ebf*.

249

250 **Coherent feed-forward circuits for cardiopharyngeal mesoderm patterning
251 and ASM fate specification.**

252 The above results indicate that *Hand-r*, *Tbx1/10* and *Ebf* require ongoing
253 FGF/MAPK activity for their successive activations in the TVCs, STVCs and ASMFs,
254 respectively. We previously showed that RNAi and/or CRISPR-mediated inhibition of

255 either *Hand-r* or *Tbx1/10* function blocks *Ebf* activation in the ASMFs, where both
256 *Hand-r* and *Tbx1/10* expressions are maintained (Razy-Krajka et al., 2014; Tolkin and
257 Christianen, 2016; Wang et al., 2013). Therefore, observations such as the loss of *Ebf*
258 expression upon *FoxF>dnFGFR* electroporation could be due to an early loss of *Hand-r*
259 and/or *Tbx1/10*. We used epistasis assays to systematically test whether early regulators
260 mediate the effects of FGF/MAPK on later gene expression and ASM fate specification,
261 or whether FGF/MAPK signaling acts both upstream and in parallel to early regulators
262 in a more complex regulatory circuit.

263 We first revisited the regulatory relationships between FGF/MAPK, *Hand-r* and
264 *Tbx1/10* in late TVCs and early STVCs. We validated single guide RNAs (sgRNAs) for
265 CRISPR/Cas9-mediated mutagenesis of *Hand-r* (Table S1; (Gandhi et al., 2017)), and
266 determined that *Hand-r* function is necessary for *Tbx1/10* activation in the STVCs
267 (Figure 4A). Co-expression of a modified *Hand-r* cDNA containing wobble base
268 mutations that disrupt the sgRNA protospacer adjacent motif (PAM; *Hand-r*^{PAMmis})
269 rescued *Tbx1/10* expression in the STVCs, indicating that *Tbx1/10* down-regulation in
270 this CRISPR "background" is specifically due to *Hand-r* loss-of-function (Figure 4A). To
271 further probe if *Hand-r* activity is necessary for FGF/MAPK-dependent *Tbx1/10*
272 expression, we used gain of M-Ras function in a *Hand-r* CRISPR "background".
273 Whereas, misexpression of the constitutively active M-Ras^{G22V} caused ectopic *Tbx1/10*
274 expression, concomitant loss of *Hand-r* function diminished both endogenous and
275 ectopic *Tbx1/10* expression in the STVC and FHP, respectively (Figure 4A). Although,
276 remaining ectopic activation could still be observed, possibly because M-Ras^{G22V} could
277 boost *Hand-r* expression in heterozygous cells where CRISPR/Cas9 disrupted only one
278 copy of the gene. This data indicate that *Hand-r* is necessary for FGF/MAPK-induced
279 activation of *Tbx1/10*.

280 To further probe the epistatic relationships between *Hand-r* and MAPK signaling
281 upstream of *Tbx1/10*, we attempted to rescue *Tbx1/10* expression in U0126-treated
282 embryos, by over-expressing *Hand-r* with the TVC-specific *FoxF* enhancer. Neither did
283 *Hand-r* over-expression cause ectopic *Tbx1/10* activation (in the FHPs), nor was it
284 sufficient to rescue *Tbx1/10* expression in 15hpf STVCs (Figure 4B). Taken together,
285 these data indicate that both *Hand-r* and MAPK activities are required to activate
286 *Tbx1/10* in the STVCs. These results also imply that MAPK signaling is restricted to the
287 STVC independently of *Hand-r* activity, which suffice to explain the STVC-specific
288 activation of *Tbx1/10*.

289

290 Next, we investigated the epistatic relationship between FGF/MAPK, *Hand-r*, and
291 *Tbx1/10* upstream of *Ebf* in the ASMFs. We first used previously validated CRIPSR/Cas9
292 reagents targeting the *Tbx1/10* coding region (Tolkin and Christiaen, 2016), to confirm
293 that B7.5-lineage-specific loss of *Tbx1/10* function inhibited *Ebf* activation, and verified
294 that this effect could be rescued by over-expression of a CRISPR/Cas9-resistant *Tbx1/10*
295 cDNA, expressed with a minimal TVC-specific *FoxF* enhancer (Figure 4C;
296 *Tbx1/10*^{PAMmis}). In these rescue experiments, we observed ectopic *Ebf* activation in the
297 SHP, as previously described when driving *Tbx1/10* expression with a TVC-specific *FoxF*
298 enhancer (Wang et al., 2013). As explained below, this ectopic activation could be
299 attributed to a precocious expression of *Ebf* in the STVCs (Figure 4E). To test whether
300 *Tbx1/10* was also required for ectopic *Ebf* expression in response to MAPK activation, we
301 combined CRISPR/Cas9-mediated *Tbx1/10* knockout with constitutive MAPK activation
302 using the M-Ras^{G22V} mutant and observed a significant inhibition of both endogenous
303 and ectopic *Ebf* expression in the 18hpf ASMF and SHP, respectively (Figure 4C). Taken
304 together, these results show that *Tbx1/10* function is necessary for FGF/MAPK-induced
305 expression of *Ebf* in the ASMFs.

306 To further test whether *Tbx1/10* acts in parallel and/or downstream of MAPK to
307 activate *Ebf*, we combined gain of *Tbx1/10* function with perturbations of FGF/MAPK
308 signaling and assayed *Ebf* expression. We realized that *FoxF*-driven misexpression of
309 *Tbx1/10* caused precocious *Ebf* activation in 15hpf STVCs (Figure 4D, E). This precocious
310 expression remained remarkably patterned, suggesting that STVC-restricted FGF/MAPK
311 activity prevented *Ebf* expression in the dpERK-negative, small median FHPs (Figures
312 1B, 4E, S1). Indeed, co-expression of both *Tbx1/10* and M-Ras^{G22V} caused both
313 precocious and ectopic *Ebf* expression in the 15hpf medial and lateral TVC derivatives,
314 which would be FHPs and STVCs in control embryos, respectively. This data confirms
315 that *Tbx1/10* misexpression does not suffice to cause ectopic *Ebf* expression in the FHPs,
316 because the latter presumably lack FGF/MAPK activity, as is the case in control embryos.

317 U0126-mediated MEK inhibition from 12 to 15hpf, i.e. after the onset of
318 *FoxF>Tbx1/10* misexpression, further confirmed that MAPK activity is required in
319 parallel to *Tbx1/10* for precocious *Ebf* activation in 15hpf STVCs (Figure 4D, E). Taken
320 together, these results indicate that *Tbx1/10* and MAPK are both required to activate *Ebf*
321 in the cell cycle following that of *Tbx1/10* onset.

322

323 Since *Hand-r* expression is maintained in the ASMF, and CRISPR/Cas9- or RNAi-
324 mediated *Hand-r* knockdown blocked both *Tbx1/10* (Figure 4A) and *Ebf* expression
325 (Razy-Krajka et al., 2014), we reasoned that *Hand-r* could also act both upstream and in
326 parallel to *Tbx1/10* for *Ebf* activation. To test this possibility, we assayed *Ebf* expression
327 in 18hpf ASMF following defined perturbations of *Hand-r* and *Tbx1/10*. As expected,
328 CRISPR/Cas9-mediated *Hand-r* mutagenesis strongly inhibited *Ebf* expression, and this
329 effect could be rescued by a CRISPR-resistant *Hand-r* cDNA (Figure 4F). To test
330 whether this effect was mediated by a loss of *Tbx1/10* expression, we attempted to rescue
331 the *Hand-r* loss-of-function by over-expressing *Tbx1/10* using the *FoxF* enhancer. As

332 explained above, *FoxF*-mediated *Tbx1/10* misexpression caused precocious and ectopic
333 *Ebf* expression in larvae co-electroporated with control sgRNAs (Figure 4D, E, F). By
334 contrast, combining loss of Hand-r function with *Tbx1/10* misexpression inhibited both
335 the endogenous and ectopic *Ebf* expression (Figure 4F), indicating that Hand-r is also
336 required in parallel to *Tbx1/10* for *Ebf* activation in the ASMFs.

337 Taken together, these analyses of the epistatic relationships between FGF/MAPK
338 signaling, *Hand-r*, *Tbx1/10* and *Ebf* suggest that coherent feed-forward circuits govern
339 the sequential activation of *Hand-r*, *Tbx1/10* and *Ebf* in response to continuous but
340 progressively restricted FGF/MAPK inputs (Figure 4G), thus linking spatial patterning to
341 the temporal deployment of the regulatory cascade leading to localized *Ebf* activation
342 and pharyngeal muscle specification.

343

344 **The cell cycle entrains the temporal deployment of the cardiopharyngeal
345 gene regulatory network.**

346 In principle, the feed-forward circuit described above is sufficient to explain the
347 successive activations of *Hand-r*, *Tbx1/10* and *Ebf*. However, *Tbx1/10* and *Ebf* do not
348 turn on until after oriented and asymmetrical divisions of the TVCs and STVCs,
349 respectively. Notably, even when we misexpressed *Tbx1/10* in the TVCs, *Ebf* was
350 activated only after TVC division and in the lateral-most cells, where FGF/MAPK
351 signaling is normally maintained (Figures 1B, 4E). This sequence of events -divisions
352 followed by gene activation- is paramount in the cardiopharyngeal mesoderm, as it
353 permits the birth of first and second heart precursors, whose fates are antagonized by
354 *Tbx1/10* and *Ebf* (Razy-Krajka et al., 2014; Stolfi et al., 2010; Wang et al., 2013).
355 Therefore, we sought to investigate the role(s) of the cell cycle in controlling the timing of
356 *Tbx1/10* and *Ebf* activations.

357 We first evaluated the effects of cytochalasin B, a classic inhibitor of cytokinesis
358 widely used to study cell fate specification in ascidians (Figure 5A; (Whittaker, 1973)).
359 Treatments starting before TVC divisions (12 hpf) did not block *Tbx1/10* or *Ebf*
360 expression in embryos fixed after their normal onset at either 16 or 19hpf, respectively
361 (Figure 5B). Similarly, treatment starting between the first and second asymmetric
362 divisions (15hpf) did not block localized *Ebf* expression at 19hpf (Figure 5B). This
363 indicates that *Tbx1/10* and *Ebf* activations occur by default in the absence of cytokinesis,
364 most likely because FGF/MAPK signaling persists throughout the shared cytoplasm.
365 This data thus illustrates how the spatial restriction of FGF/MAPK signaling, following
366 cell divisions, leads to the localized activations of *Tbx1/10* and *Ebf*, and permits the
367 emergence of first and second cardiac precursors.

368 Cytochalasin treatments usually lead to the formation of polynucleated cells (e.g.
369 Figure 5B, middle panel), because the cell cycle and nucleokinesis continue in these
370 artificial endoreplicating cells. To alter cell cycle progression more comprehensively, and
371 specifically in the cardiopharyngeal lineage, we used genetically encoded inhibitors of
372 cell cycle transitions: Cdkn1b.a and Cdkn1b.b (also known as Noto16), the ortholog of
373 which is a potent inhibitor of the G1/S transition in the ascidian species *Halocynthia*
374 *roretzi* (Kuwajima et al., 2014), and Wee1, a G2/M inhibitor, as previously described
375 (Dumollard et al., 2017). We used the TVC-specific *FoxF* enhancer to misexpress these
376 negative regulators of cell cycle progression, monitored cell divisions and assayed
377 *Tbx1/10* expression at 15hpf, when control TVCs have divided and the lateral-most
378 STVCs normally express *Tbx1/10*. Each perturbation efficiently inhibited TVC divisions,
379 such that only two cells were visible on either side of the embryos (Figure 5C). In these
380 delayed TVCs, *Tbx1/10* expression was strongly reduced compared to control STVCs
381 (Figure 5C; compare to Figure 4A, B). However, approximately 40% of the delayed TVCs
382 expressed *Tbx1/10* to variable extents. This suggests that the cardiopharyngeal

383 regulatory network can qualitatively unfold independently of cell cycle progression, but
384 the latter is necessary for *Tbx1/10* expression to its wild-type levels.

385 We next used the STVC-specific *Tbx1/10 T12* enhancer, to misexpress Cdknib.a,
386 Noto16 and Wee1, and assay *Ebf* expression at later stages. Inhibitors of the G1/S
387 transition failed to block STVC divisions (data not shown), most likely because *T12*-
388 driven products did not accumulate quickly enough to interfere with the G1/S transition
389 in STVCs (this cell cycle lasts only ~2 hours compared to ~6 hours for the TVC
390 interphase), suggesting that the G1 phase is too short for *T12*-driven gene products to
391 accumulate before the G1/S transition. Therefore, we focused the analyses of *Ebf*
392 response to cell cycle perturbations on misexpression of the G2/M inhibitor Wee1.
393 Preliminary analyses of 18hpf larvae, fixed approximately 2 hours after the documented
394 onset of *Ebf* expression in ASMFs (Razy-Krajka et al., 2014), indicated that *Ebf* can turn
395 on in arrested STVCs that failed to divide upon Wee1 misexpression (Figure 5D).

396 Because ~30% of the embryos showed variable expression, as was the case for
397 *Tbx1/10* in the previous experiment, we reasoned that perturbations of the G2/M
398 transition could alter the dynamics of *Ebf* upregulation. We investigated this possibility
399 using embryos fixed every 30 minutes between 15.5hpf and 18hpf, when cells transition
400 from a late *Tbx1/10+; Ebf-* STVC state to a committed *Ebf+, Mrf+* ASMF state (Razy-
401 Krajka et al., 2014; Wang et al., 2013). First, we observed that the proportion of embryos
402 with conspicuous ASMFs increased from ~20% to >90% between 15.5 and 16.5 hpf in
403 control embryos (Figure 4E). By contrast, Wee1-expressing cells had divided in only
404 ~35% of the embryos by 16.5hpf, and that proportion gradually increased to ~70% by
405 18hpf (Figure 4E), indicating that Wee1 misexpression strongly delays cell cycle
406 progression, blocking cell divisions in a substantial fraction of embryos.

407 Focusing on ASMFs, we found that the proportion of *Ebf+* cells in control embryos
408 progressively increased from ~20% showing "weak" expression at 15.5hpf to >90%

409 showing "strong" expression by 18hpf (Figure 5F; see Figure 5D for examples of "weak"
410 and "strong" expression). This semi-quantitative analysis revealed an under-appreciated
411 dynamic at the onset of *Ebf* expression, which appears to take at least one hour to be
412 "strongly" expressed in >75% of newborn ASMFs (Figure 4F).

413 To evaluate the impact of Wee1-induced mitosis inhibition on *Ebf* accumulation, we
414 focused on undivided STVCs at each time point (hence the lower numbers in Figure 4F
415 compare to Figure 4E). By 17hpf, *wee1*-expressing delayed STVCs showed "strong" *Ebf*
416 expression in comparably high proportions of embryos. However, these proportions
417 were significantly lower at 16 and 16.5hpf (Chi-square tests, $P=0.002$ and $P=0.0003$,
418 respectively), with ~1.5 and ~1.2 times less "strongly" expressing cells than in the control
419 distributions (hypergeometric tests, $P=0.0005$ and $P=0.0001$, respectively). These semi-
420 quantitative data suggests that the cardiopharyngeal network can eventually unfold and
421 lead to high levels of *Ebf* expression independently of cell divisions, albeit with a delay
422 revealing that cell divisions probably entrain *Ebf* upregulation in early ASMFs.

423

424 **Transition from a MAPK-dependent to a MAPK-independent and
425 autoregulatory mode of *Ebf* expression in early ASMFs.**

426 Given the semi-quantitative nature of our analysis, and the relatively subtle effects
427 observed on *Ebf* dynamics, we sought to further probe the mechanisms that regulate the
428 onset and upregulation of *Ebf* expression in early ASMFs, and the biological significance
429 for cell-fate specification. Since we observed a progressive accumulation of *Ebf* mRNAs,
430 and a transition from a MAPK-dependent onset to a MAPK-independent maintenance of
431 *Ebf* transcription (Figure 3I, J), we reasoned that the window of MAPK-dependence
432 might coincide with the accumulation of *Ebf* mRNAs between 16 and 17hpf. To test this
433 possibility, we treated embryos with the MEK inhibitor U0126 at successive time points,
434 assayed ongoing transcription using intronic probes and counted the numbers of *Ebf*

435 transcribing cells (Figure 6A). This analysis revealed that *Ebf* transcription gradually lost
436 its sensitivity to MAPK inhibition between 16 and 17hpf, i.e. during the first hour of the
437 ASMF cycle when *Ebf* mRNAs normally accumulate (as shown in Figure 5E, F).

438 Because *Ebf* transcription becomes independent from MAPK by the time *Ebf* mRNA
439 have accumulated to "high" levels, and because *Ebf* expression lasts for several days in
440 the progeny of the ASMFs, we reasoned that autoregulation might suffice to maintain
441 high levels of *Ebf* mRNA past the MAPK-dependent onset. To test this possibility, we
442 misexpressed the *Ebf* coding sequence using the STVC-specific *T12* enhancer as
443 described (Tolkin and Christiaen, 2016). Assaying endogenous *Ebf* transcription using
444 intronic probes demonstrated that, in addition to its normal expression in the ASMFs,
445 *Ebf* misexpression caused precocious and ectopic activation of the endogenous locus in
446 the STVCs, and in the MAPK-negative SHPs, respectively (Figure 6C-F). This result
447 suggests that *Ebf* transcription bypasses both requirements for cell-division coupling and
448 MAPK inputs if high levels of *Ebf* gene products are present in the cell.

449 We reasoned that, if high levels of *Ebf* expression can promote its own transcription
450 independently of MAPK signaling, then *Ebf* misexpression should be sufficient to rescue
451 a chemical inhibition of MAPK at a critical stage. We tested this possibility by combining
452 *Ebf* misexpression using the STVC-specific *T12* enhancer and U0126 treatments starting
453 at 16hpf, which normally block *Ebf* expression (Figure 6A, D-F). We observed that
454 transcription of the endogenous *Ebf* locus became independent of early MAPK activity
455 upon misexpression of an *Ebf* cDNA, further supporting the notion that high levels of
456 *Ebf* expression suffice to maintain *Ebf* transcription independently of MAPK activity.

457

458 A potentially important implication of this transient MAPK-dependence is to
459 render *Ebf* expression initially reversible. For instance, *Ebf* occasionally turns on
460 precociously in the STVCs of a small proportion of embryos (Figure S4). Given the

461 powerful anti-cardiogenic effects of *Ebf* (Razy-Krajka et al., 2014; Stolfi et al., 2010),
462 persistent *Ebf* expression would have dramatic consequences for SHP development
463 (Wang et al., 2013). However, because MAPK activity is excluded from the SHPs, and the
464 early phase of *Ebf* expression depends upon continuous MAPK activity, we surmise that
465 *Ebf* cannot be maintained in the SHPs. For instance, when embryos from the same
466 electroporated batch were fixed at the time of early U0126 treatment (i.e. 15.75 and
467 16.25hpf) and ~4 hours later, at 20hpf, and assayed for *Ebf* transcription using intronic
468 probes, initially wild-type patterns of *Ebf* transcription could not be maintained (Figure
469 S5A). This suggests that, although *Ebf* can be activated precociously in a MAPK-
470 dependent manner, its expression shuts off in the SHPs upon MAPK inhibition following
471 STVC division.

472 We further addressed the interplay between cell division, MAPK signaling and *Ebf*
473 expression. We reasoned that, if cell divisions entrain *Ebf* accumulation and the
474 transition to a MAPK-independent autoregulatory mode, then delaying STVC divisions
475 should extend the period of MAPK-dependent *Ebf* transcription. We tested this
476 possibility by expressing *Wee1* under the control of the STVC-specific *T12* enhancer, and
477 treated embryos with U0126 at 17hpf, which inhibited the maintenance of *Ebf*
478 transcription in only 15% to 20% of the control embryos (Figures 6A, S5B). The
479 proportion of embryos showing U0126-sensitive *Ebf* transcription increased to almost
480 50% upon *T12>Wee1* expression (Figure S5B), which is consistent with our hypothesis
481 that inhibiting the G2/M transition delayed the accumulation of *Ebf* gene products thus
482 postponing the transition from a low level/MAPK-dependent to an high level/MAPK-
483 independent and self-activating mode of *Ebf* regulation.

484 Taken together these data lead us to propose a model for *Ebf* regulation whereby
485 Hand-r, Tbx1/10, ongoing MAPK signaling and cell-cycle-regulated transcriptional
486 input(s) govern the onset and initial accumulation of *Ebf* gene products during the first

487 hour of the ASMF cycle, whereas the maintenance of *Ebf* expression relies primarily on
488 MAPK-independent autoactivation, following initial accumulation (Figure 7).

489 **Discussion**

490 Here, we demonstrated that the progressive restriction of FGF/MAPK signaling
491 follows asymmetric cell divisions of multipotent progenitors and patterns the ascidian
492 cardiopharyngeal mesoderm in space and time. This leads to the localized expression of
493 *Hand-r*, *Tbx1/10* and *Ebf* in fate-restricted pharyngeal muscle precursors, and their
494 concomitant exclusion for first and second heart precursors. We show that coherent
495 feedforward circuits encode the successive activations of *Hand-r*, *Tbx1/10* and *Ebf*,
496 whereas cell divisions entrain the progression of this regulatory sequence and thus
497 define the timing of gene expression. Finally, we provide evidence that the initiation of
498 *Ebf* expression depends on MAPK activity in early ASMF, until Ebf accumulation permits
499 MAPK-independent auto-activation. Given the potent anti-cardiogenic, and pro-
500 pharyngeal muscle effects of Ebf (Razy-Krajka et al., 2014; Stolfi et al., 2010), we surmise
501 that the latter switch corresponds to the transition from a cardiopharyngeal multipotent
502 state to a committed pharyngeal muscle identity.

503

504 **Spatial patterning by localized maintenance of FGF/MAPK signaling.**

505 Our results demonstrate that MAPK signaling is maintained only in the lateral-most
506 daughter cells following each asymmetric division of multipotent cardiopharyngeal
507 progenitors - the TVCs and STVCs. This asymmetric maintenance is necessary and
508 sufficient for the progressive and localized deployment of the pharyngeal muscle
509 network. Notably, the TVCs themselves are initially induced by similar polarized
510 FGF/MAPK signaling coincidental to asymmetric cell divisions of their mother cells, aka
511 the B8.9 and B8.10 founder cells (Davidson et al., 2006). Detailed analyses have since
512 indicated that asymmetrical maintenance of sustained FGF/MAPK signaling involves
513 intrinsic Cdc42-dependent polarity of the founder cells, which promotes polarized cell-
514 matrix adhesion of the prospective TVC membrane to the ventral epidermis. The latter

515 differential integrin-mediated adhesion promotes localized MAPK activation, leading to
516 TVC induction (Cooley et al., 2011; Norton et al., 2013). It has been proposed that
517 adhesion- and caveolin-dependent polarized FGFR recycling during mitosis accounts for
518 the localized activation of MAPK in the prospective TVCs (Cota and Davidson, 2015).
519 Whereas similar mechanisms could in principle account for asymmetric maintenance of
520 FGF/MAPK signaling in STVCs and ASMFs, this has not been formally tested and there
521 are notable differences opening the possibility that other mechanisms may be at work:
522 during TVC induction, MAPK signaling is maintained in the smaller daughter cell that
523 contacts the epidermis, whereas in the following divisions, MAPK activity persists in the
524 larger daughter cells and all cells maintain contact with the epidermis (Nicole Kaplan
525 and Lionel Christiaen, data not shown). Moreover, using an FGFR::mKate2 fusion
526 protein similar to that used in previous studies, we could not observed a marked
527 polarized distribution of FGFR molecules to the lateral-most cells (the STVCs and
528 ASMFs; Yelena Bernadskaya and Lionel Christiaen, data not shown). However, the fact
529 that constitutively active forms of M-Ras and Mek1/2 were sufficient to bypass the loss of
530 MAPK activity, and impose pharyngeal muscle specification, indicates that differential
531 FGF/MAPK activity is regulated upstream of M-Ras. Further work is needed to elucidate
532 the cellular and molecular mechanisms governing the spatiotemporal patterns of
533 FGF/MAPK signaling in the cardiopharyngeal mesoderm. In particular, it will be
534 important to disentangle the relative impacts of extrinsic (i.e. tissues, contacts) vs.
535 intrinsic (i.e. asymmetric cell division) effects onto FGF/MAPK signaling and the
536 downstream transcriptional inputs.

537

538 **Transcriptional effects of differential FGF/MAPK signaling.**

539 Because differential FGF/MAPK signaling rapidly impacts cell-specific gene
540 expression, we surmise that transcriptional effectors are dynamically regulated. For

541 instance, even though we have not formally identified the downstream DNA-binding
542 transcription factor (see discussion below), it would be conceivable that the
543 phosphorylated forms of either transcriptional effector persist through cell division upon
544 maintenance of FGF/MAPK activity. However, we have shown that continuous MAPK
545 activity is needed following each division. Therefore, we must invoke elusive
546 phosphatase activities, such as dual-specificity phosphatases (DUSPs; (Patterson et al.,
547 2009), which would reset transcriptional effectors to a dephosphorylated state, thus
548 rendering steady-state FGF/Ras/MAPK inputs necessary.

549 Systematic dephosphorylation of FGF/MAPK transcriptional effectors is likely to be
550 particularly important for heart fate specification. For instance, whole genome analyses
551 indicate that heart-specific *de novo* gene expression requires MAPK inhibition (Wang et
552 al., 2017). Although the molecular mechanisms remain elusive, one simple possibility is
553 that, lest fate-restricted heart precursors inhibit MAPK activity, they will activate
554 *Tbx1/10* and *Ebf*, which will block the cardiac program (Razy-Krajka et al., 2014; Stolfi et
555 al., 2010; Wang et al., 2013). Finally, we previously proposed that repressor inputs from
556 *Nk4* are needed in the second heart precursors to avoid ectopic activation of *Ebf* (Wang
557 et al., 2013). The observation that *Nk4* transcripts are detected in all cardiopharyngeal
558 cells opened the question as to how *Ebf* would escape repression by *Nk4* in the ASMFs.
559 Differential MAPK activity offers an intriguing possibility: for instance, *Nk4/Nkx2-5*-
560 mediated repression in other species involves the co-repressor Groucho/TLE (Choi et al.,
561 1999), which is strongly expressed in the cardiopharyngeal mesoderm (Razy-Krajka et
562 al., 2014); and, in flies, MAPK-mediated phosphorylation of Groucho inhibits its
563 repressor function (Cinnamon et al., 2008; Cinnamon and Paroush, 2008; Hasson et al.,
564 2005). Therefore, it is possible that persistent MAPK signaling dampens Groucho/TLE-
565 mediated repressive inputs on cell-specific regulatory genes like *Ebf*. Future studies will

566 determine whether such mechanisms provide bistable switches underlying MAPK-
567 dependent fate choices in the cardiopharyngeal mesoderm.

568

569 **Temporal deployment of the pharyngeal muscle network**

570 The localized and successive activation of *Tbx1/10* and *Ebf* in STVCs, and ASMFs,
571 respectively, are important features of the cardiopharyngeal network that permit the
572 emergence of diverse cell fates: first and second heart precursors, and atrial siphon
573 muscle precursors. Experimental misexpression of *Ebf* throughout the cardiopharyngeal
574 mesoderm suffice to inhibit heart development (Razy-Krajka et al., 2014; Stolfi et al.,
575 2010), illustrating how important it is for *Ebf* expression to be restricted to the ASMF,
576 once the first and second heart precursors are born and have terminated MAPK activity.

577 Our analyses indicate that the sequential activations of *Hand-r*, *Tbx1/10* and *Ebf* is
578 encoded in the feed-forward structure of this sub-circuit, whereas the continuous
579 requirement for MAPK inputs and their progressive exclusion from heart progenitors
580 restrict the competence to activate *Tbx1/10* and *Ebf* to the most lateral cells, after each
581 division. Our model implies that each gene may directly respond to transcriptional
582 inputs from MAPK signaling. We have not formally identified the transcription factors(s)
583 that mediate the transcriptional response to FGF/MAPK signaling. However,
584 multipotent cardiopharyngeal progenitors express *Ets1/2* and *Elk*, two common
585 transcriptional effectors of FGF/MAPK signaling in *Ciona* (Bertrand et al., 2003;
586 Christiaen et al., 2008; Davidson et al., 2006; Gainous et al., 2015). Moreover, *Ets1/2*
587 has been implicated in the initial FGF/MAPK-dependent induction of multipotent TVCs
588 (Christiaen et al., 2008; Davidson et al., 2006), and its expression is also progressively
589 restricted to the lateral-most progenitors following each division (Razy-Krajka et al.,
590 2014). Taken together, *Ets1/2* and, to some extend, *Elk* are intriguing candidate
591 transcriptional effectors of FGF/MAPK signaling in cardiopharyngeal development.

592 The binding preferences of Ets-family factors have been extensively studied in *Ciona*,
593 and they do not depart markedly from conserved Ets-family binding sites with a GGAW
594 core (Bertrand et al., 2003; Farley et al., 2015; Farley et al., 2016; Gueroult-Bellone et al.,
595 2017; Khoueiry et al., 2010). Putative Ets-family binding sites in the TVC-specific *Hand-*
596 *r* enhancer are conserved between *Ciona intestinalis* and its sibling species *C. robusta*
597 and *C. savignyi*, and necessary for its activity in reporter assays (Woznica et al., 2012).
598 Similarly, minimal STVC and ASM enhancers for *Tbx1/10* and *Ebf*, respectively, contain
599 conserved putative Ets-family binding sites, although their function has not been tested
600 ((Razy-Krajka et al., 2014; Wang et al., 2013) and data not shown). Taken together, these
601 observations suggest that the proposed feed-forward sub-circuit involves direct
602 transcriptional inputs from FGF/MAPK-regulated Ets-family factors on the
603 cardiopharyngeal enhancers of *Hand-r*, *Tbx1/10* and *Ebf*.

604

605 Whereas the regulatory architecture of the MAPK; Hand-r; *Tbx1/10*; *Ebf* sub-circuit
606 explains the sequence of activation events, it is also crucial for its correct deployment,
607 and the generation of diverse cell identities, that genes are not fully activated before
608 successive cell divisions. While divisions are not absolutely required for *Ebf* to eventually
609 turn on, cell cycle progression appears to entrain the deployment of this network,
610 especially for *Tbx1/10* and *Ebf* activation in STVCs and ASMFs, respectively. These
611 observations imply that, while the network can eventually unfold, its intrinsic dynamic is
612 slower than observed. This allows first and second heart precursors to be born prior to
613 the onset of *Tbx1/10* and *Ebf*, respectively. The latter sequence is essentially for the heart
614 progenitors to escape the anti-cardiogenic effects of *Tbx1/10* (Wang et al., 2013), and *Ebf*
615 (Razy-Krajka et al., 2014).

616 Initial *Ebf* expression in early ASMFs is also labile and MAPK-dependent for
617 approximately one hour. This continued requirement for MAPK inputs ensures that, in

618 the rare instances when *Ebf* expression starts in the multipotent STVC progenitors
619 and/or expands to the nascent SHPs, inhibition of MAPK shuts off *Ebf* expression before
620 it reaches the levels needed for commitment to an ASM fate. Indeed, our results indicate
621 that, once *Ebf* mRNAs have accumulated to high levels, its expression becomes auto-
622 regulative and MAPK-independent. We surmise that this transition coincides with a
623 fundamental switch from a multipotent cardiopharyngeal state to a committed
624 pharyngeal muscle identity.

625 From this standpoint, the observed entrainment of *Ebf* expression by the cell cycle
626 can be seen as acceleration of the transition to commitment following asymmetric
627 division of multipotent progenitors. Although the mechanisms remain elusive, it is likely
628 that this requires the M/G1 transition, as the G1 phase has been shown to be particularly
629 conducive to the expression of fate-specific regulators in mammalian pluripotent stem
630 cells (Dalton, 2015; Pauklin et al., 2016; Pauklin and Vallier, 2013; Soufi and Dalton,
631 2016).

632

633 **Conserved dual effects of FGF/MAPK signaling on heart development in 634 chordates**

635 Previous studies highlighted how FGF/MAPK signaling is necessary along side Mesp
636 during early cardiac development in *Ciona* (Christiaen et al., 2008; Davidson, 2007;
637 Davidson et al., 2006), and how this early requirement also exists in vertebrates (Abu-
638 Issa et al., 2002; Alsan and Schultheiss, 2002; Barron et al., 2000; Brand, 2003; Reifers
639 et al., 2000; Zaffran and Frasch, 2002). We now know that these early FGF/MAPK
640 inputs induce and maintain multipotent cardiopharyngeal states in *Ciona*, including the
641 *Tbx1/10+* multipotent progenitors that eventually produce the second heart lineage
642 ((Razy-Krajka et al., 2014; Stolfi et al., 2010; Wang et al., 2013; Wang et al., 2017), and
643 this study). Similarly, in vertebrates, regulatory interplay between *Fgf8* and *Fgf10*

644 signaling and *Tbx1* is required for development of both pharyngeal arch and second
645 heart field derivatives, presumably in part by maintaining an undifferentiated and
646 proliferative state (Abu-Issa et al., 2002; Aggarwal et al., 2006; Brown et al., 2004; Chen
647 et al., 2009; Hu et al., 2004; Ilagan et al., 2006; Kelly and Papaioannou, 2007; Park et
648 al., 2006; Park et al., 2008; Vitelli et al., 2002b; Watanabe et al., 2010; Watanabe et al.,
649 2012). Notably, FGF signaling acts in successive phases, and its inhibition is necessary
650 for final myocardial specification and differentiation (Hutson et al., 2010; Marques et al.,
651 2008; Tirosh-Finkel et al., 2010; van Wijk et al., 2009). Conversely, continued FGF
652 signaling beyond the multipotent mesodermal progenitor stages was shown to promote
653 smooth muscle and epicardial differential in the heart (Hutson et al., 2010; van Wijk et
654 al., 2009), and also myoblast specification and/or skeletal muscle differentiation in the
655 head, with the expression of FGF ligands being maintained in the pharyngeal arches
656 (Bothe et al., 2011; Buckingham and Vincent, 2009; Michailovici et al., 2015;
657 Michailovici et al., 2014; von Scheven et al., 2006). Taken together, these and our data
658 suggest that FGF/MAPK signaling plays evolutionary conserved roles during chordate
659 cardiopharyngeal development, by promoting the specification of successive mesodermal
660 and *Tbx1*+ multipotent states, and a fate-restricted non-cardiac muscle identity, while
661 MAPK inhibition is required for myocardial specification and differentiation in the first
662 and second heart field, successively.

663 **Material and methods**

664 **Animals, electroporations, and chemical treatments**

665 Gravid wild *Ciona intestinalis* type A, now called *Ciona robusta* (Pennati et al., 2015),
666 were obtained M-REP (Carlsbad, CA, USA), and kept under constant light to avoid
667 spawning. Gametes from several animals were collected separately for *in vitro* cross-
668 fertilization followed by dechorionation and electroporation as previously described
669 (Christiaen et al., 2009a, b). Different quantities of plasmids were electroporated
670 depending on the constructs. Typically, 50 µg of DNA was electroporated for NLS::lacZ
671 or plain mCherry driving constructs but only 15 µg for *Mesp-1>H2B::mCherry*. For
672 perturbation constructs, 70 µg were usually electroporated, except for
673 *Mesp>NLS::Cas9::NLS* (30 µg) and pairs of U6>sgRNA plasmids (25 µg each). U0126
674 (Cell Signaling Technology, Danvers, MA) was used at 5µM in artificial seawater from a
675 stock solution of 20mM in DMSO. Cytochalasin B (Sigma, Saint Louis, MO) was used at
676 ~3 µg/mL from a 10 mg/mL stock solution in DMSO as previously performed (Jeffery et
677 al., 2008). Control embryos were incubated in parallel with corresponding
678 concentrations of DMSO alone.

679

680 ***In situ* hybridization**

681 *In situ* hybridizations were carried out essentially as described previously (Christiaen et
682 al., 2009c; Razy-Krajka et al., 2014), using DIG labeled riboprobes, anti-DIG-POD Fab
683 fragments (Roche, Indianapolis, IN), and Tyramide Amplification Signal coupled to
684 Fluorescein (Perkin Elmer, MA). Reporters expressed in the lineage of interest were
685 marked using anti-β-galactosidase monoclonal mouse antibody (1:1000; Promega,
686 Fitchburg, WI) or anti-mCherry rabbit polyclonal antibody (1:500; BioVision 5993-100),
687 respectively targeted with anti-mouse or anti-rabbit secondary antibody coupled with

688 Alexa 648 (1:500; Invitrogen, Carlsbad, CA). The different probes used in this study were
689 described previously (Razy-Krajka et al., 2014; Stolfi et al., 2010; Wang et al., 2013).

690

691 **dpERK/mcherry double fluorescent immunostaining**

692 Samples were fixed, as for *in situ* hybridizations, in MEM-PFA with Tween 20 (0.05%)
693 but only for 30 minutes at room temperature, washed three times in PBSt (Tween 20
694 0.01%) for 10 minutes, gradually dehydrated every 10 minutes in Ethanol/PBS series
695 (33%, 50%, 80%) and Methanol 100%. Samples were then gradually rehydrated every 10
696 minutes in Methanol/PBSt series, rinsed three times in PBSt, permeabilized with PBS
697 Triton-100 (0.2%) for 30 minutes and incubated for 2 hours at room temperature with
698 anti-dpERK mouse monoclonal antibody (1:200; Sigma, Saint Louis, MO) and anti-
699 mCherry polyclonal antibody from rabbit (1:500; Biovision, Milpitas, CA) in PBS 0.01%
700 Triton-100 (T-Pbs) supplemented with 2% normal goat serum. Samples were then
701 washed three times in T-PBS and incubated in anti-mouse and anti-rabbit antibodies
702 (1 :500 each), respectively coupled with Alexa 488 and Alexa 568 (Invitrogen, Carlsbad,
703 CA), overnight at 4°C or for 2 hours at room temperature. Finally, samples were rinsed
704 three times in T-PBS for 15 minutes and mounted in Prolong Gold (Molecular Probes,
705 Eugene, OR).

706

707 **Molecular cloning**

708

709 Coding sequences for wild-type M-Ras (KH.L172.2), Mek1/2 (KH.L147.22), Cdkn1b.a
710 (Cdkn1b, KH.C14.564), and Cdkn1b.b (Noto16, KH.S643.6) were PCR-amplified from
711 cDNA libraries prepared by reverse transcription of total RNA from mixed
712 developmental stages. Insertion of the products into expressing vectors was performed
713 using regular restriction/ligation or In-fusion (Clontech, Mountain View, CA) procedure.
714 Oligonucleotide directed mutagenesis or two-step overlap PCRs were used to generate

715 the point mutated forms M-Ras^{G22V} and Mek^{S220E,S216D} from the corresponding wild-type
716 sequences. We also used oligonucleotide directed mutagenesis to generate mismatches in
717 the PAM sequences adjacent to the sgRNA targets for Hand-r (153C>T 574C>T for
718 Hand-r^{PAMmis}) and Tbx1/10 (325G>A and 579G>A for Tbx1/10^{PAMmis}). Due to the absence
719 of a correct PAM sequence (NGG, (reverse complement CCN)), overexpressed Hand-
720 r^{PAMmis} and Tbx1/10^{PAMmis} are resistant to the Cas9 nuclease activity. Primer sequences
721 are listed in Supplementary Table 1.

722
723 **CRISPR/Cas9-mediated loss of Hand-r function**

724 The pair of single guide RNA (sgRNA) targeting Tbx1/10 (sgTbx1/10) has been validated
725 previously (Tolkin and Christiaen, 2016). Rescue of the Tbx1/10 loss-of-function was
726 achieved by TVC-specific overexpression of Tbx1/10^{PAMmis} driven by a *FoxF* enhancer
727 (*FoxF-1>Tbx1/10^{PAMmis}*). For Hand-r loss of function, sgRNAs were first designed to
728 avoid genomic off-targets and tested as described (Gandhi et al., 2017). In short, sgRNA
729 expressing cassettes (U6>sgRNA) were assembled by single step overlap PCR. Individual
730 PCR products (~25 µg) were electroporated with EF1a>NLS::Cas9::NLS (30µg) ,
731 Myod905>Venus (50 µg), driving ubiquitous expression of Cas9 and a widely expressed
732 fluorescent reporter construct, respectively. Efficient electroporation was confirmed by
733 observation of fluorescence before genomic DNA extraction around 16 hpf (18°C) using
734 QIAamp DNA Micro kit (Qiagen, German Town, MD). Mutagenesis efficacy of individual
735 sgRNAs, as a linear function of Cas9-induced indel frequency, was estimated from
736 electrophoregrams following Singer sequencing of the targeted regions amplified from
737 extracted genomic DNA by PCR. Result of the relative quantification of the indel
738 frequency (“corrected peakshift” of 22% and 24%) was considered high enough for both
739 sgRNAs targeting Hand-r, which were finally selected. The corresponding cassettes were
740 cloned into plasmid for repeated electroporations to study the loss of function of Hand-r.

741 Rescue of Hand-r loss-of-function was achieved by overexpression of Hand-r^{PAMmis}
742 driven by a FoxF TVC specific enhancer (FoxF-1>Hand-r^{PAMmis}). In order to control the
743 specificity of the CRISPR/Cas9 system, sgRNAs targeting *Neurogenin*, a gene not
744 expressed in the TVC and their progeny, was electroporated in parallel. Sequences of the
745 DNA targets and oligonucleotides used for the sgRNAs are listed in Supplementary Table
746 1.

747

748 **Observation and imaging**

749 Samples were usually scored under a DM2500 epifluorescent microscope (Leica
750 Microsystems, Wetzlar, Germany). Imaging was performed using a TCS SP8 X inverted
751 confocal microscope equipped with a white light laser, AOBS and HyD detectors (Leica
752 Microsystems).

753

754 **Acknowledgement**

755 We thank Robert Kelly (Université Aix-Marseille, CNRS, France) for feedbacks on the
756 manuscript. We are grateful to Wei Wang, Nicole Kaplan, Claudia Racioppi and Alberto
757 Stolfi for collaborative inputs throughout the project. We thank Farhana Salek and
758 Kristyn Millan for technical support. This project was funded by NIH/NHLBI R01 award
759 HL108643, and trans-Atlantic network of excellence award 15CVD01 from the Leducq
760 Foundation to L.C.

761

762 **Figures**

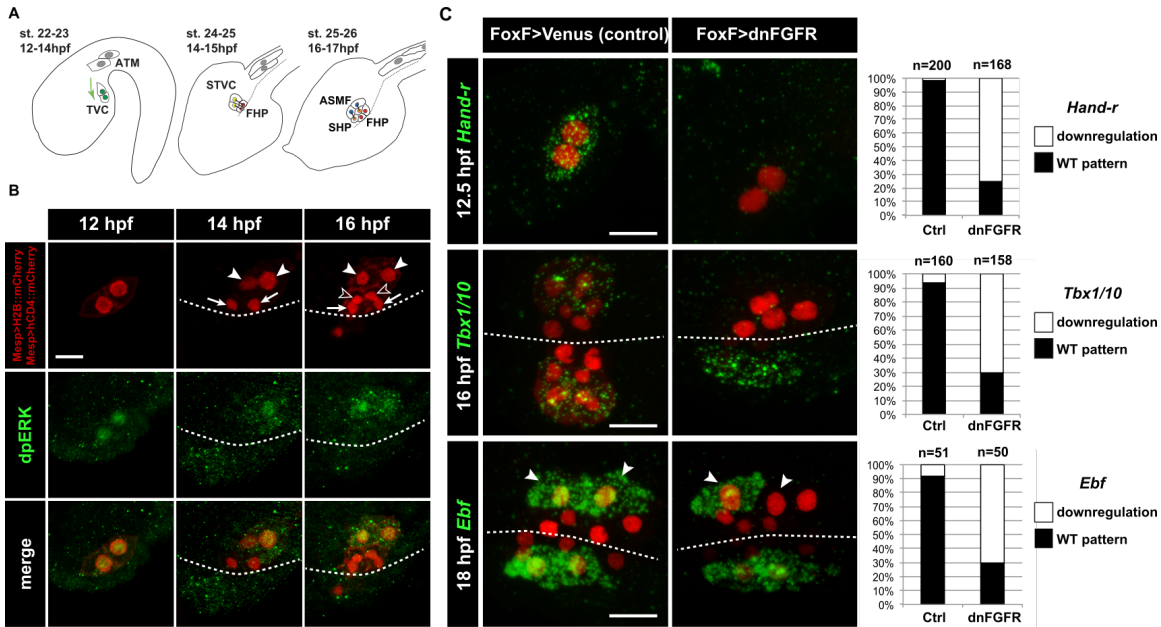
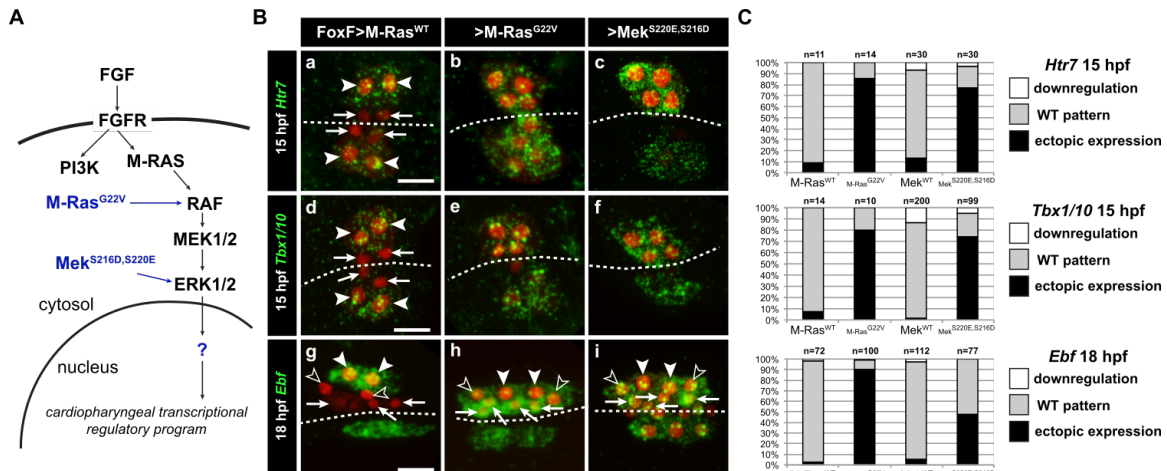
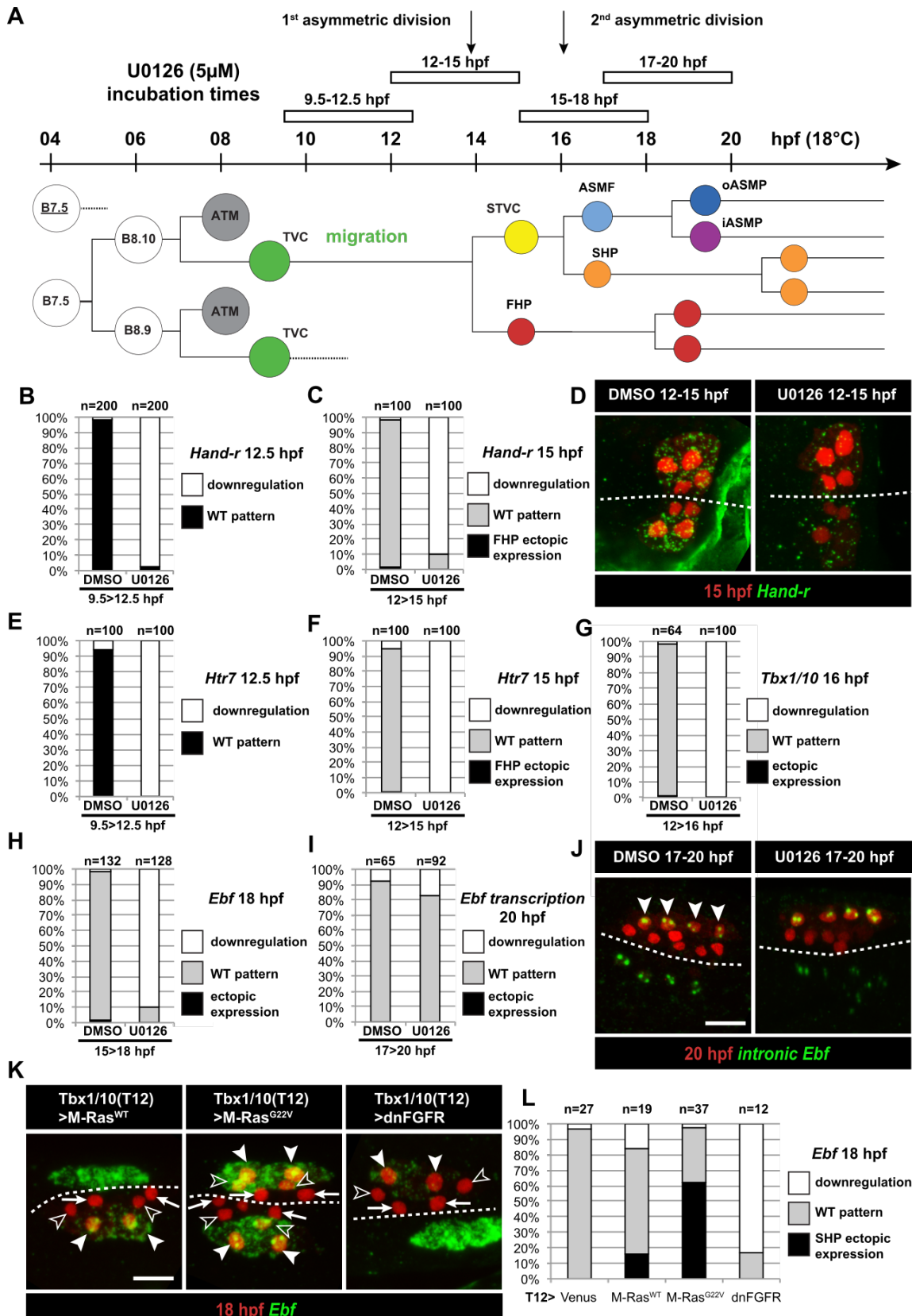


Figure 1. Spatio-temporal restriction of ERK activity reflects FGF requirement for the specification of cardiopharyngeal progenitors. (A) Schematic of *Ciona* development showing asymmetric cell divisions and resulting cell fates of the cardiopharyngeal mesoderm (CPM). Embryonic and larval stages (St) according to (Hotta et al., 2007) with hours post fertilization (hpf) at 18°C. Anterior tail muscle (ATM, gray), trunk ventral cell (TVC, green), secondary TVC (STVC, green), first heart precursor (FHP, red), second heart precursor (SHP, orange), atrial siphon founder cell (ASMF, blue). Black bars link sister cells. Dashed lines: ventral midline. The first stage presents a quasi-lateral view while the second and third stages present quasi-ventral views. Anterior is to the left. Scale bar, 50 µm. (B) ERK activity visualized by anti-dpERK antibody (green). TVCs and their progeny are marked by mCherry driven by *Mesp* and revealed by anti-mCherry antibody (red). H₂B::mCherry and hCD4::mCherry accumulate in the nuclei and at the cell membrane, respectively. Arrowheads indicate STVCs and ASMFs at 14 and 16 hpf, respectively. Arrows indicate FHPs and open arrowheads mark SHPs. Anterior to the left. Scale bar, 10 µm. See also Figure S1 for broader time series of dpERK immunostaining in the B7.5 lineage. (C, D) TVC-specific overexpression of dnFGFR induces loss of expression of key lateral CPM markers visualized by *in situ* hybridization. (C) Representative expression patterns of key CPM genes (*Hand-related*, *Tbx1/10*, *Ebf*) in control embryos (control, electroporated with *FoxF(TVC):bpFOG-1>Venus*) and TVC-specific dnFGFR expression (electroporated with *FoxF(TVC):bpFOG-1>dnFGFR::mCherry*) individuals. TVCs and progeny are marked with *Mesp>NLS::lacZ* (red). Loss of expression in half of the TVC progeny, as presented for *Ebf*, is assumed to be due to left-right mosaicism. Arrowheads mark the ASMFs. Anterior is to the left. Scale bar, 10 µm. (D) Corresponding histograms with the phenotype proportions. For simplicity, loss of gene expression in half or all of the TVCs and their progeny were combined in the same category. "n" corresponds to the number of individual halves documented per condition.



787
788 **Figure 2. Constitutively active M-Ras and MEK are sufficient to impose a pharyngeal muscle**
789 **fate in the cardiopharyngeal lineage.** (A) Diagram of the FGF/MAPK transduction pathway with
790 constitutive activation by M-Ras^{G22V} and MEK^{S216D,S220E} mutants. (B) Expression patterns of markers of the
791 lateral TVC progeny, *Htr7* (a, b, c), *Tbx1/10* (d, e, f) and *Ebf* (g, h, i), visualized by *in situ* hybridization
792 following TVC-specific over-expression of M-Ras^{WT} (as control), M-Ras^{G22V} and MEK^{S216D,S220E}. M-Ras^{WT}
793 overexpression (a, d, g) does not alter the wild-type spatial expression patterns of *Htr7*, *Tbx1/10* and *Ebf* in
794 lateral TVC derivatives (STVC and ASMF) and excluded from the median heart precursors. TVC-specific
795 over-expression of M-Ras^{G22V} (b, e, h) or MEK^{S216D,S220E} (c, f, i) induces ectopic expression of STVC and/or
796 ASMF markers (*Htr7*, *Tbx1/10* and *Ebf*) in the more median cells, that normally form cardiac precursors.
797 Solid arrowheads indicate STVCs and ASMFs at 15 and 18 hpf, respectively. Arrows indicate FHPs and open
798 arrowheads mark SHPs. At 18 hpf, the FHPs start dividing or have divided into 4 cells. Anterior to the left.
799 Scale bar, 10 μ m. (C) Corresponding histograms: Larvae with TVC-specific over-expression of MEK^{WT} retain
800 the wild-type expression patterns. For simplicity, ectopic expressions in half to all of the cardiac precursors
801 were combined in the same phenotype category. "n" corresponds to the number of embryo halves
802 documented per condition. See also Figure S2.



804
805
806

Figure 3. Temporal requirement for MAPK activity permits the progressive deployment of the cardiopharyngeal regulatory program. (A) Summary of the CPM cell lineage showing the

807 different Uo126 treatments with regard to the timing of the cell divisions. Abbreviations and color codes as
808 in Figure 1. **(B, C)** Proportions of embryo halves with wild-type or downregulated expression of *Hand-r* at
809 12.5 hpf (B) and 15 hpf (C) following 3-hour incubations in Uo126 (with DMSO as control treatment). **(D)**
810 *Hand-r* expression visualized by *in situ* hybridization at 15 hpf in control (DMSO treated) and Uo126 treated
811 embryos. In control embryos, *Hand-r* remains expressed in the STVCs and downregulated in the FHPs. In
812 Uo126 (12-15 hpf) treated embryos, downregulation of *Hand-r* expression is observed throughout the TVC
813 progeny (STVCs and FHPs), suggesting inhibition of transcription and inheritance of remnant transcripts
814 following TVC divisions. **(E, F)** Proportions of embryo halves with wild-type or downregulated expression of
815 *Htr7* at 12.5 hpf (E) and 15 hpf (F) following 3-hour incubations in Uo126 (with DMSO as control
816 treatment). **(G)** Proportions of larvae with wild-type expression or downregulated expression of *Tbx1/10* at
817 16 hpf following 4-hour incubation in Uo126 (with DMSO as control). **(H)** Proportions of larvae with wild-
818 type or downregulated expression of *Ebf* at 18 hpf following a three hour incubation in Uo126 (with DMSO
819 as control). **(I)** Proportions of larvae with wild-type or downregulated transcription of *Ebf* at 18 hpf following
820 a 3-hour incubation in Uo126 (DMSO as vehicle control). **(J)** Pattern of nascent *Ebf* transcripts visualized by
821 *in situ* hybridization with intronic probes (green) at 20 hpf. The nuclear dots reveal the active transcription
822 sites in the four ASMPs per side in larvae, both control/DMSO- and Uo126-treated from 17 to 20 hpf. **(K)**
823 *Ebf* expression (green) in 18hpf larvae expressing control M-Ras^{WT}, constitutively active M-Ras^{G22V} or
824 dominant negative dnFGFR under the control of the T12 element, an STVC-specific *Tbx1/10* enhancer.
825 Arrows: first heart precursors (FHP); open arrowhead: second heart precursors (SHPs); closed arrowheads:
826 ASM founder cells (ASMFs); dotted line: midline. **(L)** Proportions of larvae with wild-type or downregulated
827 expression of *Ebf* at 18 hpf in larvae with Venus (control), M-Ras^{WT}, M-Ras^{G22}, or dnFGFR driven by
828 *Tbx1/10 cis*-regulatory sequence and overexpressed in the STVCs. "n" : number of individual halves
829 documented per condition.
830

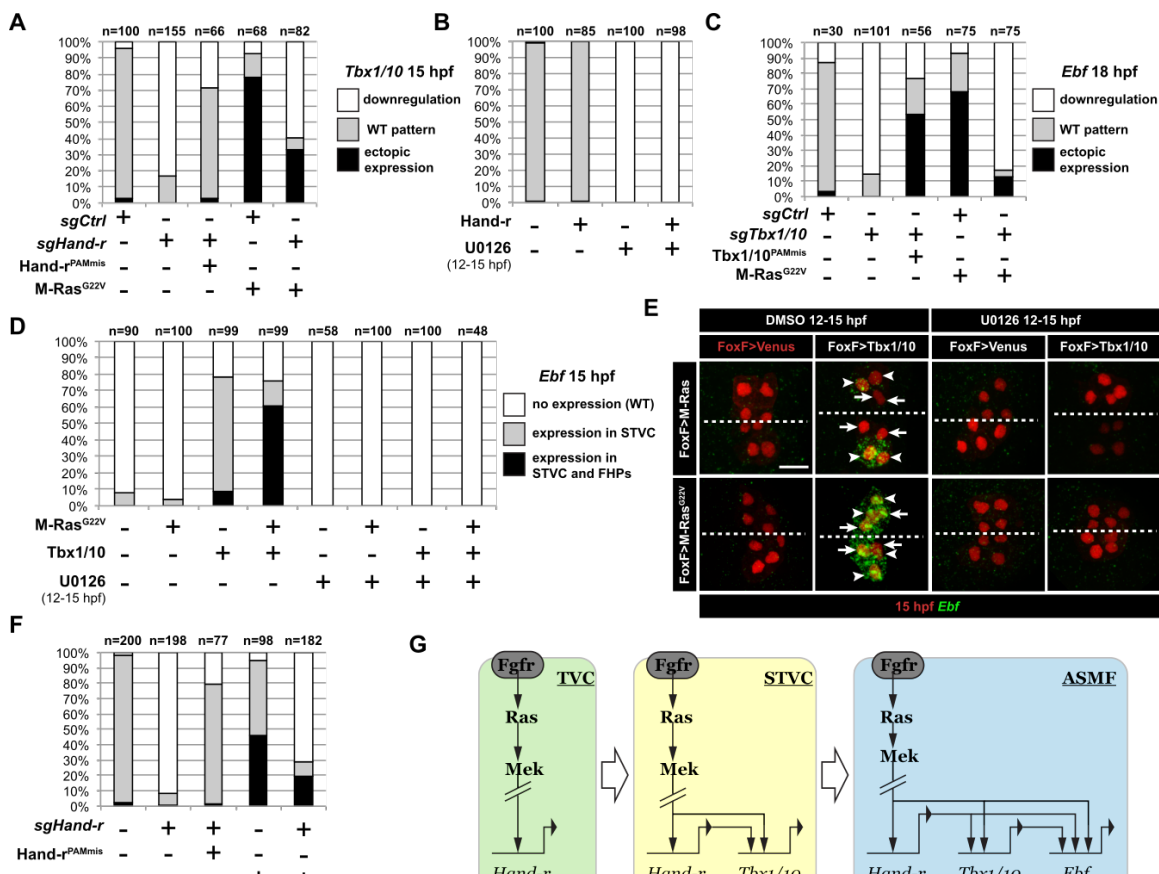


Figure 4. M-Ras/MAPK-driven feed-forward subcircuits control the successive activations of Hand-r, Tbx1/10 and Ebf. (A) Proportions of embryo halves with indicated *Tbx1/10* expression patterns following TVC-specific CRISPR/Cas9-mediated mutagenesis of *Neurogenin/Neurog* as a control (sgCtrl), and Hand-r (sgHand-r). TVC-specific overexpression of a CRISPR/Cas9-resistant form of Hand-r with mutation in the PAM sequence (*Hand-r^{PAMmis}*) rescued *Tbx1/10* expression in the sgHand-r "background". TVC-specific overexpression of a constitutively active M-Ras mutant (M-Ras^{G22V}) (control: M-Ras^{WT}) was sufficient to induce ectopic expression of *Tbx1/10* in the FHPs in sgCtrl embryos but not in sgHand-r embryos indicating that Hand-r is necessary for M-Ras-dependent activation of *Tbx1/10* transcription. (B) Proportions of embryo halves with indicated *Tbx1/10* expression patterns following TVC-specific overexpression of Hand-r or a neutral reporter (Venus) and treated from 12 to 15 hpf with the MEK inhibitor U0126 (+) or with DMSO (-) as control. Hand-r overexpression is not sufficient to rescue loss of *Tbx1/10* expression due to MAPK inhibition indicating that M-Ras/MAPK activity is required in parallel of Hand-r expression to activate *Tbx1/10* transcription in the TVC progeny. (C) *Tbx1/10* is necessary downstream of M-Ras/MAPK activity to activate *Ebf* transcription in the TVC progeny. Shown are proportions of *Ebf* expression phenotypes following TVC-specific CRISPR/Cas9-mediated loss of *Tbx1/10* function (sgTbx1/10), with *Neurog*-targeting sgRNA as control (sgCtrl). Specificity of *Tbx1/10* loss of function was validated through rescue of *Ebf* expression with TVC-specific overexpression of a CRISPR/Cas9 resistant form of *Tbx1/10* (*Tbx1/10^{PAMmis}*). Ectopic *Ebf* expression in SHPs in *Tbx1/10^{PAMmis}* larvae is explained by precocious misexpression of *Tbx1/10* in the TVC as described in Wang et al, 2013. TVC-specific overexpression of M-Ras^{G22V} (M-Ras^{G22V}), with wild type M-Ras (M-Ras^{WT}) as control, was sufficient to induce ectopic expression of *Ebf* in the cardiac precursors in sgCtrl embryos but not in sgTbx1/10 embryos indicating that *Tbx1/10* is necessary for M-Ras-dependent activation of *Ebf* transcription. (D, E) Proportions (D) and examples (E) of 15 hpf larva halves showing indicated *Ebf* expression phenotypes in sgCtrl and sgHand-r CRISPR/Cas9 conditions combined with TVC-specific overexpression of a neutral reporter (Venus), Hand-r^{PAMmis}, or *Tbx1/10*, and with MEK inhibition by U0126 (+) or not (DMSO control (-)). Arrowhead: STVCs, Arrows: FHPs, dotted line: ventral midline (F) Loss of Hand-r function impaired the ability of *Tbx1/10* to induce ectopic *Ebf* expression. For simplicity, ectopic expressions in half to all of the cardiac precursors were combined in the same phenotype category. "n": number of individual halves documented per condition. (G) Summary model of the temporal deployment of FGF/MAPK-driven feed-forward subcircuits leading to the sequential activations of *Tbx1/10* and *Ebf* in the STVCs and ASMFs, respectively.

831

832

833

834

835

836

837

838

839

840

841

842

843

844

845

846

847

848

849

850

851

852

853

854

855

856

857

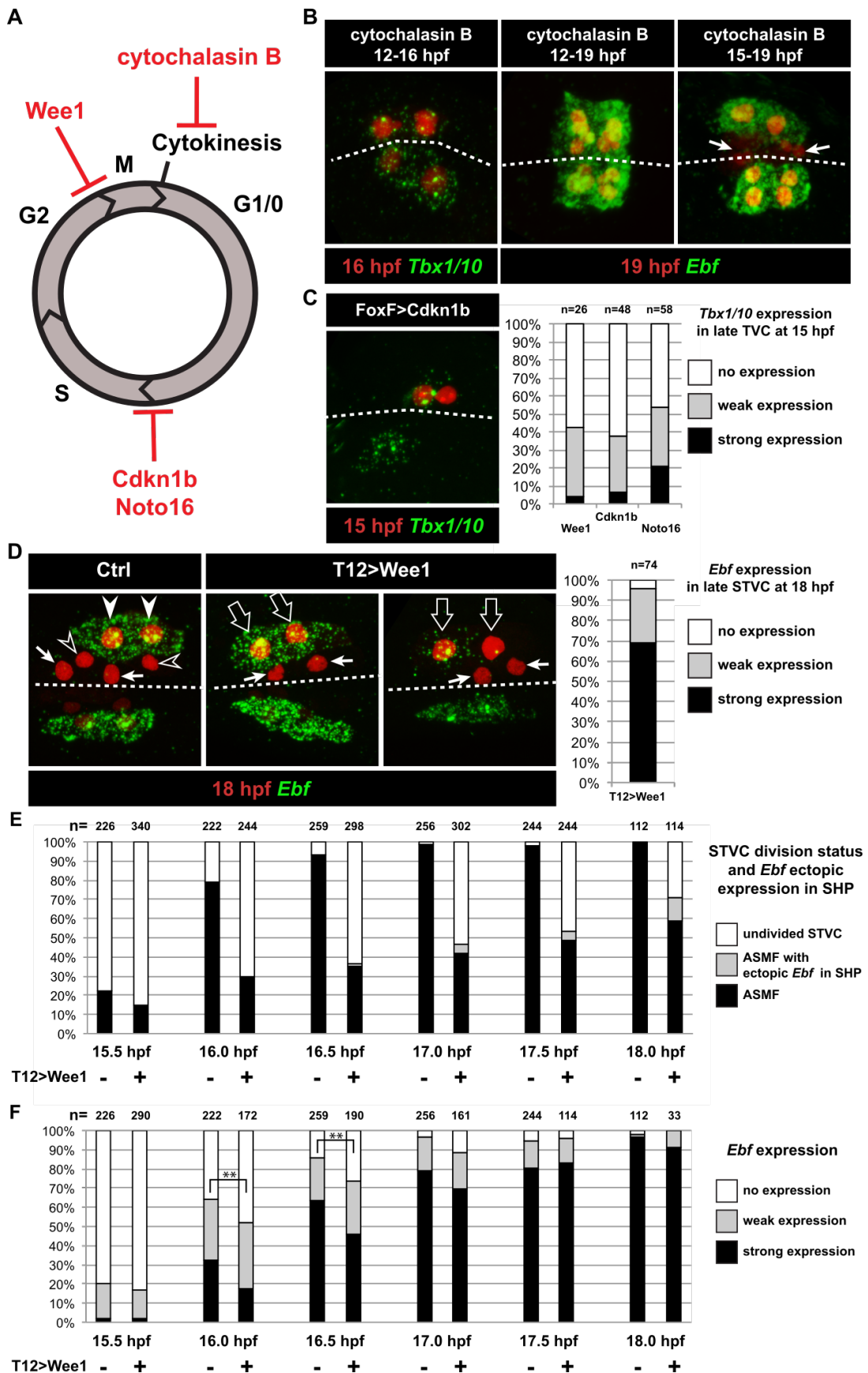
858

859

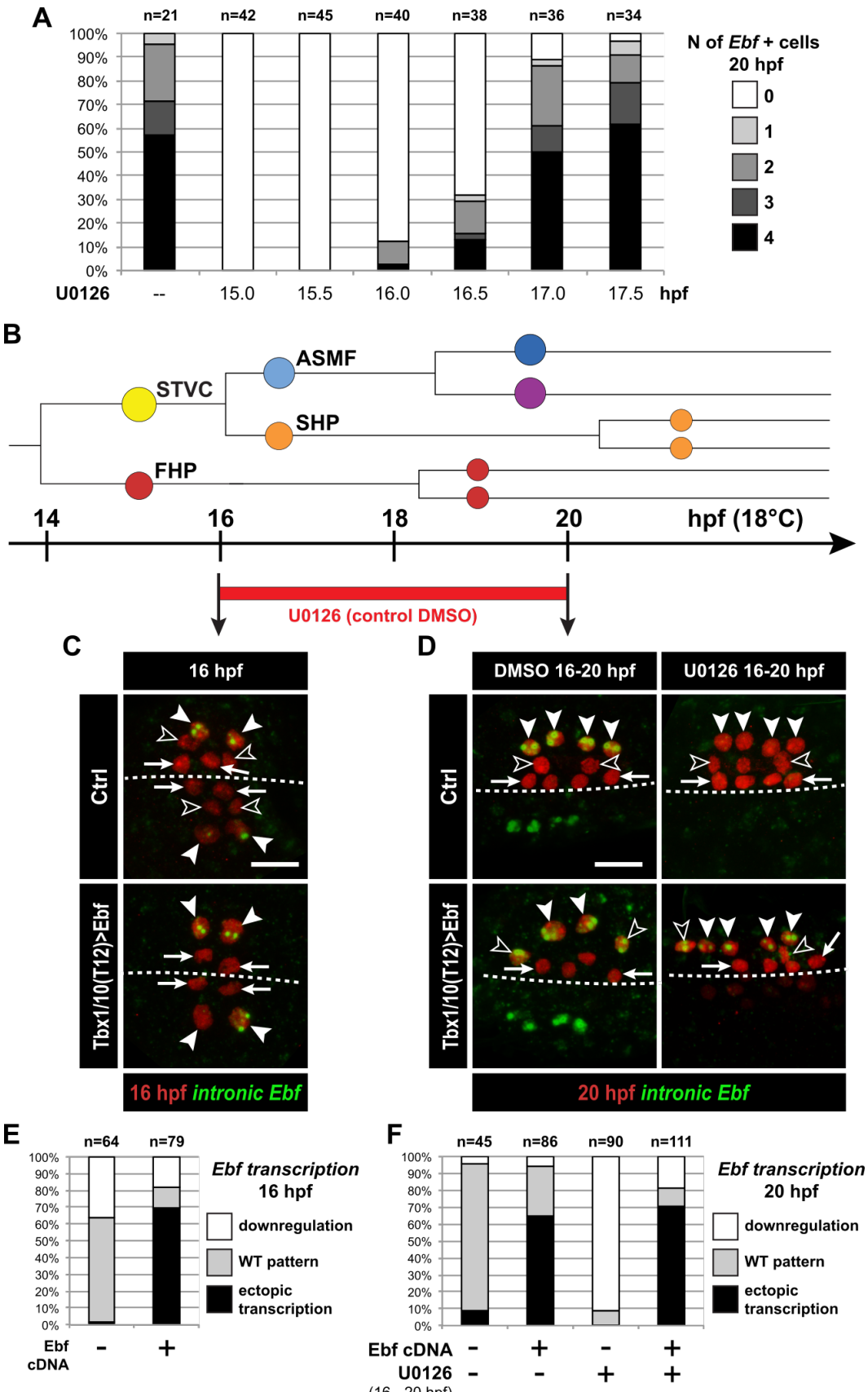
860

861

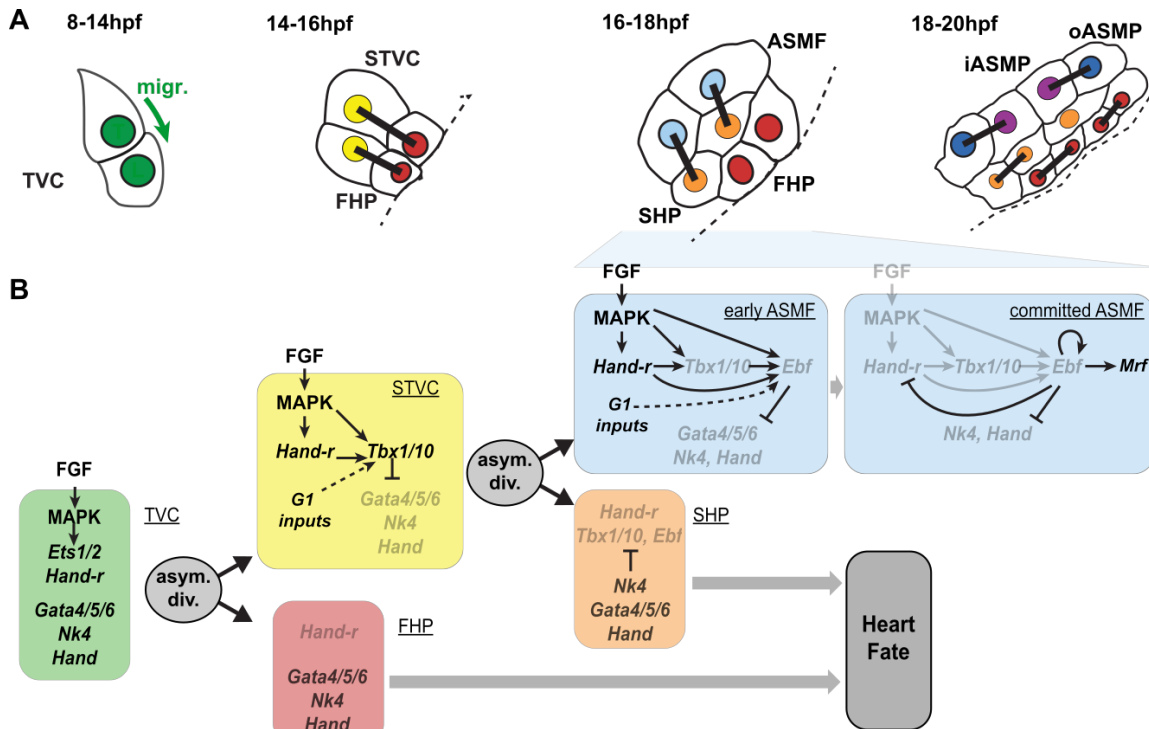
862



864
865 **Figure 5. Temporal deployment of the cardiopharyngeal network is partially coupled with cell**
866 **cycle progression.** (A) Schematic representation of the canonical eukaryotic cell cycle, and actions of the
867 perturbations used in this study. (B) *Tbx1/10* and *Ebf* expression at indicated time points, and following
868 inhibition of cytokinesis by cytochalasin B treatment at indicated time points. Note that 15 to 19hpf
869 treatment is applied AFTER the first division and birth the FHPs, which do not activate *Ebf* at 19hpf (right
870 panel, arrows). (C) Inhibition of G1/S or G2/M blocks TVC division, and reduces *Tbx1/10* expression.
871 Picture shows left-right mosaic embryo, with TVCs that have not divided on the electroporated side (marked
872 by *Mesp>H2B::mCherry*, red), one cell turned on *Tbx1/10*, but not the other. Left: the proportions of
873 embryos showing strong *Tbx1/10* expression is substantially reduced compared to control embryos (e.g.
874 Figure 1, and (Wang et al., 2013)). (D) Inhibition of G2/M in the STVCs by misexpression of Wee1 using the
875 *Tbx1/10 T12* enhancer inhibits STVC division, and has a mild impact on *Ebf* expression at 18hpf. Open
876 arrows indicate STVCs that have not divided, but express high (middle) or low (right) levels of *Ebf*. Left:
877 control larva showing high *Ebf* expression in the ASMF (closed arrowheads), but neither in the SHPs (open
878 arrowheads) nor in the FHPs (Arrows). (E) Proportions of larva halves fixed at successive time points and
879 showing undivided STVCs, or ASMFs with or without ectopic *Ebf* expression in the SHPs following STVC-
880 specific expression of the G2/M inhibitor Wee1 (+), or a control construct (-). See Figure S4C for an example
881 of ectopic *Ebf* expression in the SHPs (grey labels). Note the sharp increase in % of larva with ASMF between
882 15.5 and 16hpf, indicating that mitosis occurs primarily during this time window, but is delayed in a majority
883 of larvae upon Wee1 misexpression. (F) Proportions of larva halves with cells showing indicated *Ebf*
884 expression. The numbers (n) for cells expressing Wee1 focus on cells that have not divided (% shown in E), to
885 estimate the dynamics of *Ebf* activation in G2/M-inhibited cells. Control cells consist mostly ASMFs after
886 15.5hpf as shown in (E). Wee1 and controls distributions differ significantly only at 16 and 16.5hpf (**,
887 p<0.01 , Chi² test), suggesting that Wee1 merely delays the accumulation of *Ebf* transcripts. In all image
888 panels, dotted line : ventral midline.

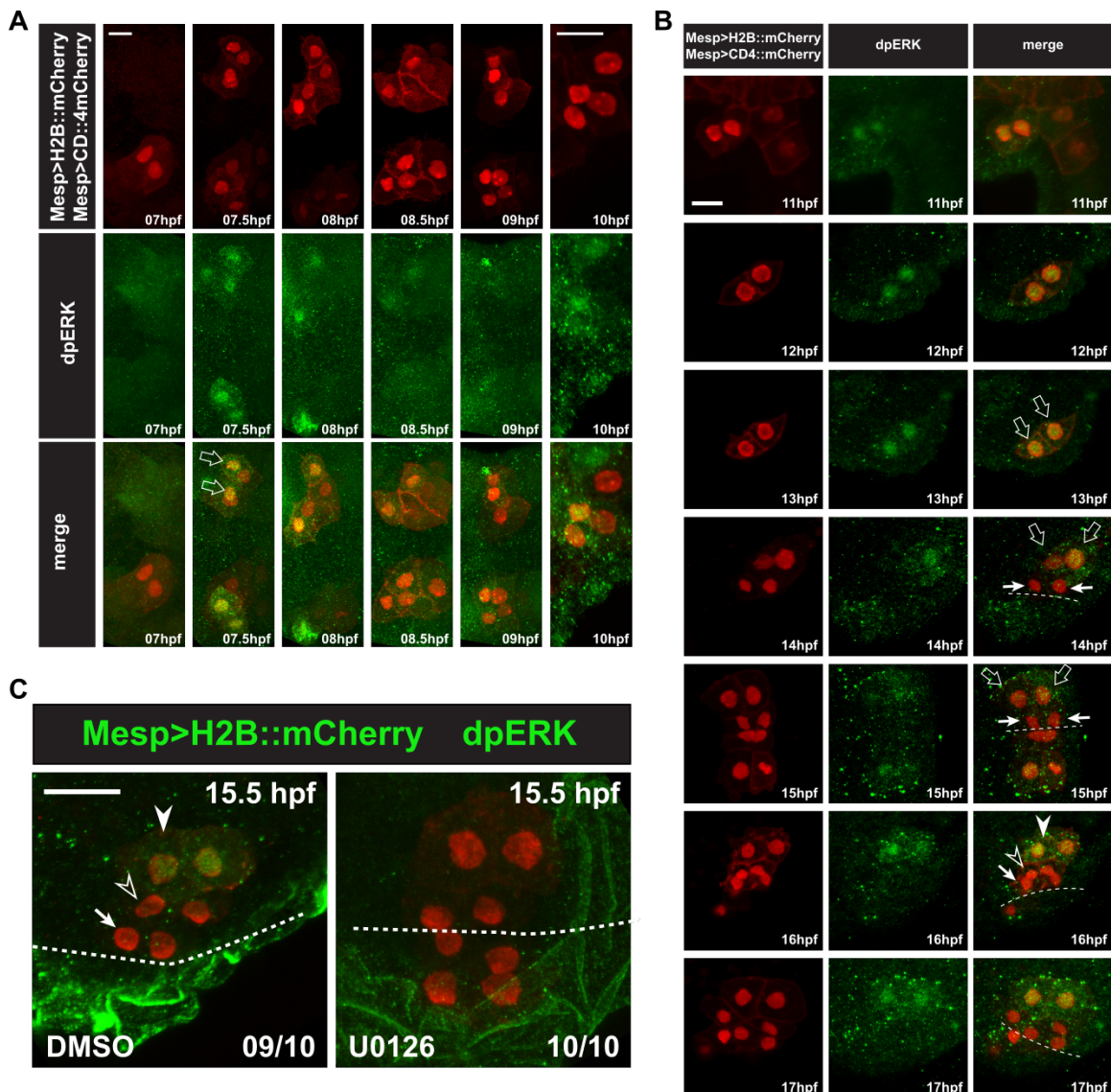


890 **Figure 6. *Ebf* regulation transitions from MAPK-dependent to autoregulatory during the early**
891 **phase of ASMF cycle.** (A) Proportions of 20hpf larva halves showing the indicated number of *Ebf*-
892 expressing cells following U0126 treatments started at the indicated time points. This indicates that, by
893 17hpf, *Ebf* expression, which started at ~16hpf, has become largely insensitive to loss of MAPK activity. (B)
894 Summary lineage diagram and time scale indicating the approximate stages for U0126 and DMSO (control)
895 treatments for the results shown in (C, D). (C) Control (Ctrl) and *Ebf*-misexpressing embryos fixed at 16hpf,
896 prior to chemical treatments, and stained for nascent transcripts with an intronic *Ebf* probe. In controls, the
897 ASMFs (solid arrowhead), but neither the SHPs (open arrowheads) nor the FHPs (arrows), actively
898 transcribe *Ebf* (green nuclear dots). In Larvae misexpressing the *Ebf* cDNA under the control of the STVC-
899 specific Tbx1/10 enhancer, divisions are delayed and STVCs (solid arrowheads) activated transcription of
900 endogenous *Ebf* loci (green nuclear dots). (D) After 4 hours, U0126 treated ASMFs no longer transcribe *Ebf*
901 (top right image, solid arrowheads), whereas control DMSO-treated ASMFs do (top left, green nuclear dots).
902 Upon misexpression of the *Ebf* cDNA in the STVCs and derivatives, ongoing *Ebf* transcription is detected at
903 20hpf in both DMSO and U0126-treated cells, and it persists in both ASMFs (solid arrowheads), and SHPs
904 (open arrowheads). (E, F). Proportions of larvae halves showing the indicated *Ebf* transcription patterns, in
905 indicated experimental conditions, as illustrated in C and D, respectively.
906



907
908
909
910
911
912
913
914
915
916
917
918
919
920
921
922
923
924
925
926
927
928
929
930
931
932
933

Figure 7. Summary model. (A) Schematic representation of cardiopharyngeal lineage cells at successive time points representing the main fate transitions. hpf: hours post-fertilization; TVC: trunk ventral cells; L: Leader T: trailer; migr.: migration; STVC: second trunk ventral cells; FHP: first heart precursors; dotted line: midline; black bars link sister cells; ASMF: atrial siphon muscle founder cells; SHP: second heart precursors; iASMP: inner atrial siphon muscle precursors; oASMP: outer atrial siphon muscle precursor (these cells correspond to stem-cell-like *Mrf*-; Notch+ precursors and *Mrf*+; Notch- differentiating myoblasts, respectively; see (Razy-Krajka et al., 2014) for details). (B) Lineage diagram and documented regulatory relationships between indicated genes and pathways, as showing here and in (Razy-Krajka et al., 2014; Wang et al., 2013). In TVCs, primed heart and ASM markers are coexpressed, and maintenance of the STVC and ASM markers requires ongoing FGF/MAPK signaling. Following the first oriented and asymmetric cell division, FGF/MAPK is maintained only in the STVCs, which permits the continued expression of Hand-r and the activation of *Tbx1/10*. Cell division, presumably through G1-specific inputs, contributes to *Tbx1/10* activation, and *Tbx1/10* function antagonizes *Gata4/5/6* expression (Wang et al., 2013). In the FHPs, termination of FGF/MAPK signaling inhibits Hand-r expression and prevents *Tbx1/10* activation. Following oriented and asymmetric division of the STVCs, FGF/MAPK signaling persists only in the ASMFs, where it permits the transient maintenance of Hand-r and *Tbx1/10*, both of which act in parallel to FGF/MAPK to activate *Ebf* expression, together with contributions from presumed G1 inputs. *Ebf* activities further antagonize the cardiac program (marked by *Gata4/5/6*, *Nk4*/*Nkx2-5* and *Hand* expression; (Razy-Krajka et al., 2014; Stolfi et al., 2010; Wang et al., 2013)). Once *Ebf* expression reaches "high levels", its regulation becomes MAPK-independent and self-activating (this study). It also feeds back negatively on early activators such as Hand-r, and promotes the expression of the muscle determinant *Mrf* (Razy-Krajka et al., 2014; Tolkin and Christiaen, 2016). We propose that this transition represents commitment to an ASM fate. In the SHPs, termination of FGF/MAPK signaling prevents maintenance of Hand-r and *Tbx1/10* expression, which, together with repressive inputs from *Nk4*/*Nkx2-5*, inhibits *Ebf* activation (Wang et al., 2013), and permits heart fate specification (Wang et al., 2017).



934
935
936
937
938
939
940
941
942
943
944
945
946
947
948
949

Figure S1. Detailed patterns of MAPK activity during early cardiopharyngeal development.
(A) MAPK activation during TVC induction. Close-up views of B7.5 lineage cells marked with Mesp>H2B::mCherry (nuclei) and Mesp>hCD4::mCherry (membranes) and immunostained for dpERK at indicated successive time points between 7 and 10hpf. DpERK staining was not detected in the founder cells at 7hpf, but increased sharply and specifically in the smaller trunk ventral cells (TVCs, open arrows) at 7.5hpf, but not in the larger anterior tail muscles (ATMs). DpERK staining persisted throughout TVC migration (see also B). **(B)** MAPK activation patterns during cardiopharyngeal fate diversification. DpERK staining was clearly detected in migrating TVCs (open arrows, 11 to 13hpf); in lateral large STVCs (open arrows, 14 to 15hpf), but not in the small median first heart precursors (FHPs, arrows, 14 to 15hpf); in the large lateral atrial siphon muscle founder cells (ASMFs, solid arrowheads, 16 to 17hpf), but neither in the FHPs (arrows), nor in the second heart precursors (SHPs, open arrowheads). **(C)** Treatment with the MEK inhibitor U0126 between abolished dpERK staining in the lateral STVCs, compared to a control treatment with DMSO. Numbers of embryos showing the presented pattern out of the total numbers of embryos are shown.

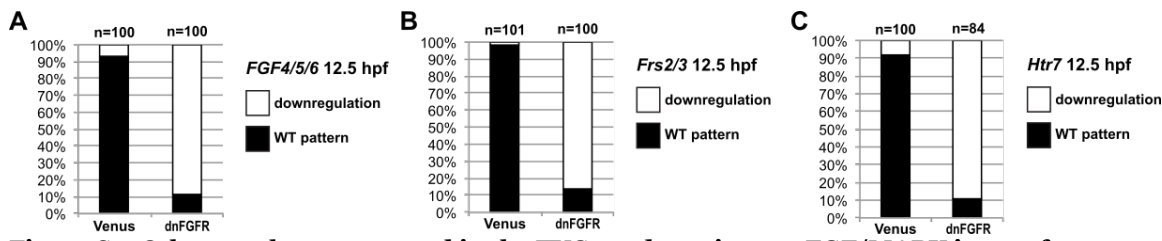
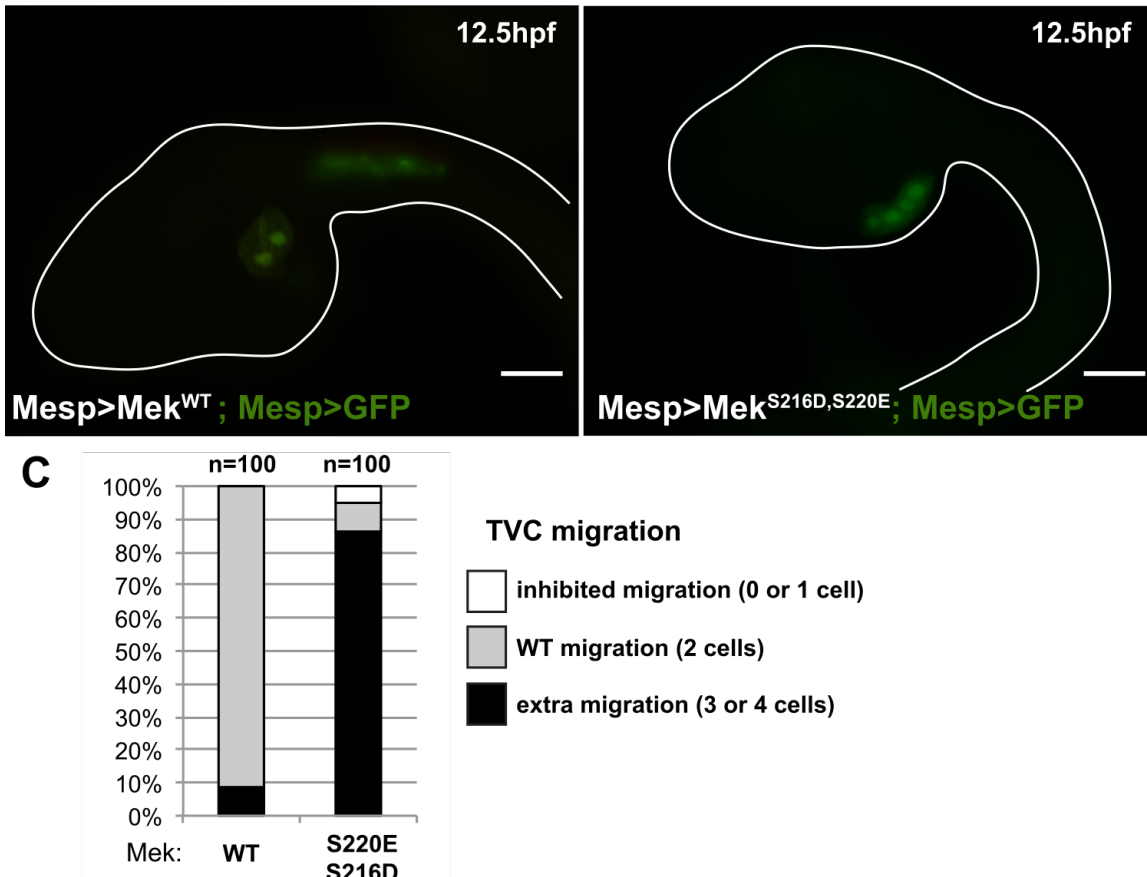
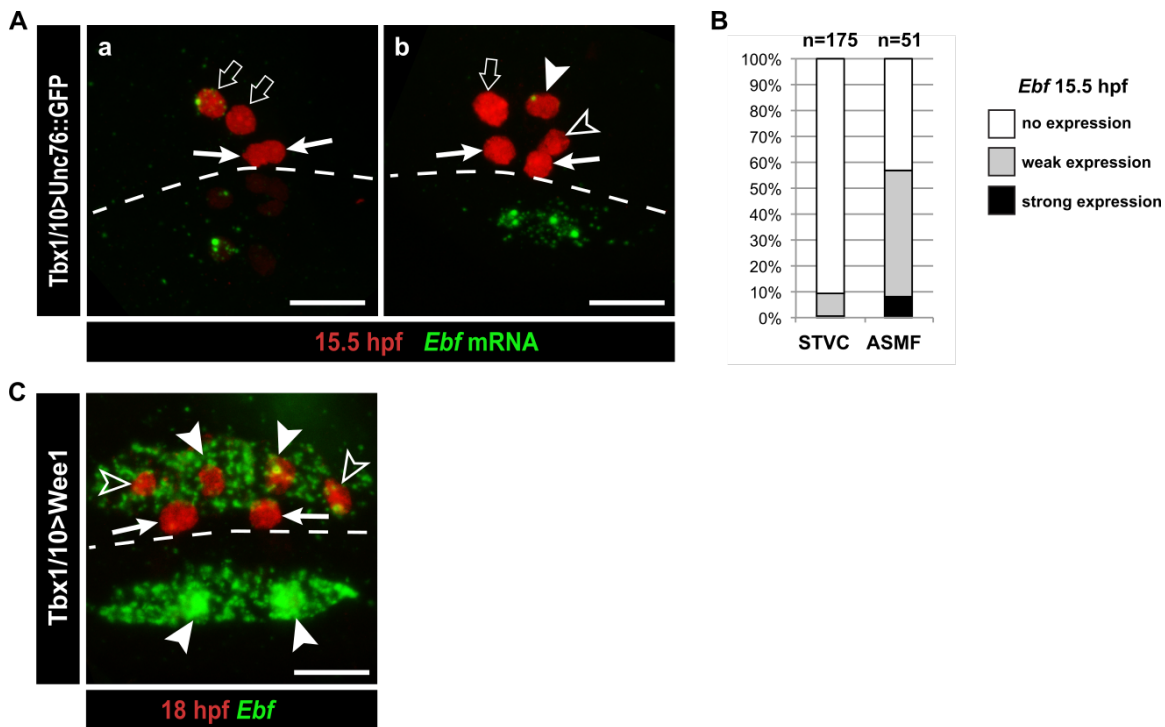


Figure S2. Other markers expressed in the TVC need continuous FGF/MAPK inputs for maintenance. All panels show the proportions of 12.5hpf embryos halves showing expression of the indicated genes in late TVCs, following electroporation of either a FoxF(TVC)>Venus control or a FoxF(TVC)>dnFGFR construct that inhibits signaling through FGFR. Wild-type pattern were first reported in (Razy-Krajka et al., 2014).

950
951
952
953
954
955
956

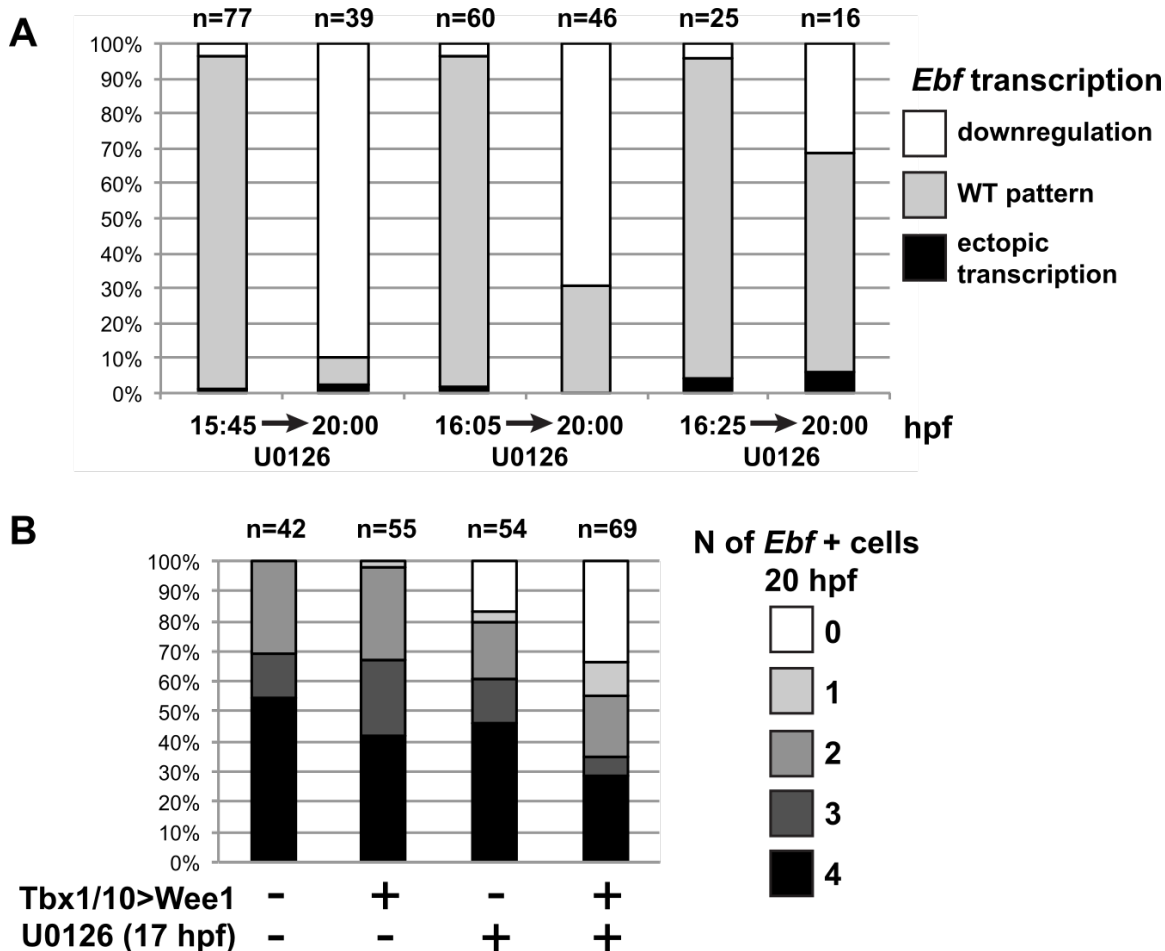


957
958 **Figure S3. The constitutively active MEK^{S216D,S220E} mutant is sufficient to impose a TVC**
959 **identity to the whole B7.5 lineage.** (A) Control late tailbud embryo showing the left side B7.5 lineage
960 expressing GFP and a MEK^{WT} control under the control of the *Mesp* enhancer. Two TVCs and two ATMs are
961 normally induced, and TVCs migrated into the trunk. (B) Late tailbud embryo showing the left side B7.5
962 lineage expressing GFP and a MEK^{S216D,S220E} mutant under the control of the *Mesp* enhancer. Four cells are
963 observed as having migrated into the trunk, indicating that they have been induced to acquire a TVC fate and
964 migrate, replicating FGF/MAPK gain-of-function phenotypes as described in (Davidson et al., 2006). (C)
965 Proportions of embryo halves showing the indicated phenotypes. Extra migration is interpreted as ectopic
966 induction of the TVC fate in all B7.5 lineage cells. Scale bar ~ 20μm.
967



968
969
970
971
972
973
974
975
976
977
978
979

Figure S4. Rare precocious activation of *Ebf* transcription in STVCs. (A) 15.5 hpf Cardiopharyngeal lineage cells expressing Mesp>H2B::mCherry (red) and control Tbx1/10>unc76::GFP construct (not visible). (A.a) Green nuclear dot indicates nascent *Ebf* transcription in an STVC (open arrow), but not the other, and not in the first heart precursors (FHP; arrow). (A.b) left pair of nuclei shows an STVC (open arrow) and an FHP (arrow), neither of which express *Ebf*, whereas the cousin ASMF (solid arrowhead) shows nascent *Ebf* transcription (green dot). Dotted line : midline. (B) Proportions of STVCs and ASMFs showing indicated *Ebf* expression patterns. Note that >90% of STVCs do not express *Ebf*, which turns on almost exclusively in ASMFs. (C) Cardiopharyngeal lineage cells with *Ebf* expression in the ASMFs (solid arrowheads), and ectopically in the SHP (open arrowheads), but not in the FHPs (arrows), following misexpression of Wee1 using the STVC-specific *Tbx1/10 T12* enhancer. Dotted line: midline.



980
981 **Figure S5. MAPK signaling is necessary for *Ebf* expression only in early ASMF, and cell cycle
982 inputs shorten the MAPK-dependent period.** (A) Proportions of larva halves showing the indicated
983 *Ebf* transcriptional activity (assayed using intronic probes). Batches of larvae expressing
984 *Mesp>H2B::mCherry* were split to be fixed for WMFISH or treated with U0126 at 3 successive time points
985 (15.75hpf, 16hpf or 16.25hpf), and the treated larvae were fixed at 20hpf. This data shows that, although all
986 batches expressed *Ebf* at the beginning of the experiment, only when MEK was inhibited later (16.25hpf) did
987 *Ebf* transcription persist in 20hpf larvae. (B) Proportions of larva halves showing the indicated numbers of
988 *Ebf*+ cells at 20hpf, following expression of the G2/M inhibitor Wee1 in the STVCs, under the control of the
989 *Tbx1/10 T12* enhancer (+). Negative controls (-) were electroporated with a *Tbx1/10(T12)>Venus* construct.
990 Larvae were also treated with U0126 (+) or DMSO (as negative control, (-)), starting at 17hpf, which
991 corresponds to the transition from a MAPK-dependent to a MAPK-independent autoregulative mode of *Ebf*
992 expression (see Figure 6A). Wee1-induced delays in cell cycle progression increased the sensitivity of late *Ebf*
993 expression to MAPK inhibition, further supporting the notion that cell divisions accelerate the transition
994 from MAPK-dependent to MAPK-independent self-activating regulation of *Ebf* transcription.
995

Primer name	primer sequence	final sgRNA
MRAS N FWD INF bpFOG-1	cacacaaaCGGCCGCaaccATGGCGACCGTGCCGAATC	GAGGCCCTGCTACCATGTGTGTTAACAGAGCTATGCTGGAAACAG
MRAS C REV INF EcoR1	gctcagctggattcTGGCCTCTAGGTGGAGCTAC	GAGGTTCGAAGTGATAATACGTTAACAGAGCTATGCTGGAAACAG
MRAS G22V TOP	GTGGTTGGCGATGTTGGTGTGGGAAG	GAGGCCCTGCTACCATGTGTGTTAACAGAGCTATGCTGGAAACAG
MRAS G22V BOT	CTTCCCAGACACCAACATGCCAACAC	GAGGCCCTGCTACCATGTGTGTTAACAGAGCTATGCTGGAAACAG
MEK1/2 N FWD Not1	caaGCGGCCGCaaccATGCCTCCTAAACGTAAGT	GAGGCCCTGCTACCATGTGTGTTAACAGAGCTATGCTGGAAACAG
MEK1/2 C REV Ecor1	cttggattcCCCATCATATTAAATCAGGTACA	GAGGCCCTGCTACCATGTGTGTTAACAGAGCTATGCTGGAAACAG
MEK MUT R	CCCTACAAACTCGTTGCCATATCGTCGATCAGTTGCCGCTCA	GAGGCCCTGCTACCATGTGTGTTAACAGAGCTATGCTGGAAACAG
MEK MUT F	CTGATCGACGATATGGCCAACCGAGTTGTAGGGACAAGATCATA	GAGGCCCTGCTACCATGTGTGTTAACAGAGCTATGCTGGAAACAG
Noto16 FWD INF bpFOG-1	acacacaaaCGGCCGCaaccATGGTCCCCCACCTCGTAC	GAGGCCCTGCTACCATGTGTGTTAACAGAGCTATGCTGGAAACAG
Noto16.2 REV INF EcoR1	GCTCAGCTGGAATTCACTTTCTGATCAATTACTTGCTTTGG	GAGGCCCTGCTACCATGTGTGTTAACAGAGCTATGCTGGAAACAG
Cdkn1B FWD INF bpFOG-1	acacacaaaCGGCCGCaaccATGGCGGACAAAAACCCCCG	GAGGCCCTGCTACCATGTGTGTTAACAGAGCTATGCTGGAAACAG
Cdkn1B REV INF EcoR1	gctcagctggattcCGTGGCACAGTATGACGTCAC	GAGGCCCTGCTACCATGTGTGTTAACAGAGCTATGCTGGAAACAG
Tbx1 G325A Mut Top	CGGCTCCGTGGAGAAGAAAATGAGCC	GAGGCCCTGCTACCATGTGTGTTAACAGAGCTATGCTGGAAACAG
Tbx1 G325A Mut Bot	CGCTCATTTCCTCTCACGGAGCCG	GAGGCCCTGCTACCATGTGTGTTAACAGAGCTATGCTGGAAACAG
Tbx1 G579A Mut Top	GAAAGATTGGTGGCCGTAGAACGAAACTGGAAATG	GAGGCCCTGCTACCATGTGTGTTAACAGAGCTATGCTGGAAACAG
Tbx1 G579A Mut Bot	CATTTCCAGTTGCTTCTACGGCCACCAATCTTC	GAGGCCCTGCTACCATGTGTGTTAACAGAGCTATGCTGGAAACAG
Hand-r C153T Mut Top	CTTGCAACCGAAAATCCACACATGGTAGC	GAGGCCCTGCTACCATGTGTGTTAACAGAGCTATGCTGGAAACAG
Hand-r C153T Mut Bot	GCTACCATGTGTGGATTTCGGTTGCAAAG	GAGGCCCTGCTACCATGTGTGTTAACAGAGCTATGCTGGAAACAG
Hand-r C574T Mut Top	GTCGCGTCCGAGTCATCGTATTATCACTTC	GAGGCCCTGCTACCATGTGTGTTAACAGAGCTATGCTGGAAACAG
Hand-r C574T Mut Bot	GAAGTGATAATACGGATGACTCGGACGCGAC	GAGGCCCTGCTACCATGTGTGTTAACAGAGCTATGCTGGAAACAG

996 **Table S1. oligonucleotides sequences**

997

998

999 **REFERENCES**

- 1000 Abu-Issa, R., Smyth, G., Smoak, I., Yamamura, K., Meyers, E.N., 2002. Fgf8 is
1001 required for pharyngeal arch and cardiovascular development in the mouse.
1002 *Development* 129, 4613-4625.
- 1003 Aggarwal, V.S., Liao, J., Bondarev, A., Schimmang, T., Lewandoski, M., Locker, J.,
1004 Shanske, A., Campione, M., Morrow, B.E., 2006. Dissection of Tbx1 and Fgf interactions
1005 in mouse models of 22q11DS suggests functional redundancy. *Human molecular genetics*
1006 15, 3219-3228.
- 1007 Alsan, B.H., Schultheiss, T.M., 2002. Regulation of avian cardiogenesis by Fgf8
1008 signaling. *Development* 129, 1935-1943.
- 1009 Barron, M., Gao, M., Lough, J., 2000. Requirement for BMP and FGF signaling
1010 during cardiogenic induction in non-precardiac mesoderm is specific, transient, and
1011 cooperative. *Developmental dynamics : an official publication of the American
1012 Association of Anatomists* 218, 383-393.
- 1013 Beh, J., Shi, W., Levine, M., Davidson, B., Christiaen, L., 2007. FoxF is essential for
1014 FGF-induced migration of heart progenitor cells in the ascidian *Ciona intestinalis*.
1015 *Development* 134, 3297-3305.
- 1016 Bertrand, V., Hudson, C., Caillol, D., Popovici, C., Lemaire, P., 2003. Neural tissue in
1017 ascidian embryos is induced by FGF9/16/20, acting via a combination of maternal GATA
1018 and Ets transcription factors. *Cell* 115, 615-627.
- 1019 Bondu, A., Lapouge, G., Paulissen, C., Semeraro, C., Iacovino, M., Kyba, M.,
1020 Blanpain, C., 2008. Mesp1 acts as a master regulator of multipotent cardiovascular
1021 progenitor specification. *Cell stem cell* 3, 69-84.
- 1022 Bothe, I., Tenin, G., Oseni, A., Dietrich, S., 2011. Dynamic control of head mesoderm
1023 patterning. *Development* 138, 2807-2821.
- 1024 Brand, T., 2003. Heart development: molecular insights into cardiac specification and
1025 early morphogenesis. *Developmental biology* 258, 1-19.
- 1026 Brown, C.B., Wenning, J.M., Lu, M.M., Epstein, D.J., Meyers, E.N., Epstein, J.A.,
1027 2004. Cre-mediated excision of Fgf8 in the Tbx1 expression domain reveals a critical role
1028 for Fgf8 in cardiovascular development in the mouse. *Developmental biology* 267, 190-
1029 202.
- 1030 Buckingham, M., Vincent, S.D., 2009. Distinct and dynamic myogenic populations in
1031 the vertebrate embryo. *Current opinion in genetics & development* 19, 444-453.
- 1032 Cai, C.L., Liang, X., Shi, Y., Chu, P.H., Pfaff, S.L., Chen, J., Evans, S., 2003. Isl1
1033 identifies a cardiac progenitor population that proliferates prior to differentiation and
1034 contributes a majority of cells to the heart. *Developmental cell* 5, 877-889.
- 1035 Chan, S.S., Hagen, H.R., Swanson, S.A., Stewart, R., Boll, K.A., Aho, J., Thomson,
1036 J.A., Kyba, M., 2016. Development of Bipotent Cardiac/Skeletal Myogenic Progenitors
1037 from MESP1+ Mesoderm. *Stem cell reports* 6, 26-34.

- 1038 Chan, S.S., Shi, X., Toyama, A., Arpke, R.W., Dandapat, A., Iacovino, M., Kang, J., Le,
1039 G., Hagen, H.R., Garry, D.J., Kyba, M., 2013. *Mesp1* patterns mesoderm into cardiac,
1040 hematopoietic, or skeletal myogenic progenitors in a context-dependent manner. *Cell*
1041 *stem cell* 12, 587-601.
- 1042 Chen, L., Fulcoli, F.G., Tang, S., Baldini, A., 2009. *Tbx1* regulates proliferation and
1043 differentiation of multipotent heart progenitors. *Circulation research* 105, 842-851.
- 1044 Choi, C.Y., Lee, Y.M., Kim, Y.H., Park, T., Jeon, B.H., Schulz, R.A., Kim, Y., 1999. The
1045 homeodomain transcription factor NK-4 acts as either a transcriptional activator or
1046 repressor and interacts with the p300 coactivator and the Groucho corepressor. *The*
1047 *Journal of biological chemistry* 274, 31543-31552.
- 1048 Christiaen, L., Davidson, B., Kawashima, T., Powell, W., Nolla, H., Vranizan, K.,
1049 Levine, M., 2008. The transcription/migration interface in heart precursors of *Ciona*
1050 *intestinalis*. *Science* 320, 1349-1352.
- 1051 Christiaen, L., Wagner, E., Shi, W., Levine, M., 2009a. Electroporation of transgenic
1052 DNAs in the sea squirt *Ciona*. *Cold Spring Harbor protocols* 2009, pdb prot5345.
- 1053 Christiaen, L., Wagner, E., Shi, W., Levine, M., 2009b. Isolation of individual cells
1054 and tissues from electroporated sea squirt (*Ciona*) embryos by fluorescence-activated cell
1055 sorting (FACS). *Cold Spring Harbor protocols* 2009, pdb prot5349.
- 1056 Christiaen, L., Wagner, E., Shi, W., Levine, M., 2009c. Whole-mount *in situ*
1057 hybridization on sea squirt (*Ciona intestinalis*) embryos. *Cold Spring Harbor protocols*
1058 2009, pdb prot5348.
- 1059 Cinnamon, E., Helman, A., Ben-Haroush Schyr, R., Orian, A., Jimenez, G., Paroush,
1060 Z., 2008. Multiple RTK pathways downregulate Groucho-mediated repression in
1061 *Drosophila* embryogenesis. *Development* 135, 829-837.
- 1062 Cinnamon, E., Paroush, Z., 2008. Context-dependent regulation of Groucho/TLE-
1063 mediated repression. *Current opinion in genetics & development* 18, 435-440.
- 1064 Cooley, J., Whitaker, S., Sweeney, S., Fraser, S., Davidson, B., 2011. Cytoskeletal
1065 polarity mediates localized induction of the heart progenitor lineage. *Nature cell biology*
1066 13, 952-957.
- 1067 Cota, C.D., Davidson, B., 2015. Mitotic Membrane Turnover Coordinates Differential
1068 Induction of the Heart Progenitor Lineage. *Developmental cell* 34, 505-519.
- 1069 Cowley, S., Paterson, H., Kemp, P., Marshall, C.J., 1994. Activation of MAP kinase
1070 kinase is necessary and sufficient for PC12 differentiation and for transformation of NIH
1071 3T3 cells. *Cell* 77, 841-852.
- 1072 Dalton, S., 2015. Linking the Cell Cycle to Cell Fate Decisions. *Trends in cell biology*
1073 25, 592-600.
- 1074 Davidson, B., 2007. *Ciona intestinalis* as a model for cardiac development. *Seminars*
1075 in cell & developmental biology 18, 16-26.

- 1076 Davidson, B., Levine, M., 2003. Evolutionary origins of the vertebrate heart:
1077 Specification of the cardiac lineage in *Ciona intestinalis*. *Proceedings of the National
1078 Academy of Sciences of the United States of America* **100**, 11469-11473.
- 1079 Davidson, B., Shi, W., Beh, J., Christiaen, L., Levine, M., 2006. FGF signaling
1080 delineates the cardiac progenitor field in the simple chordate, *Ciona intestinalis*. *Genes &*
1081 *development* **20**, 2728-2738.
- 1082 Davidson, B., Shi, W., Levine, M., 2005. Uncoupling heart cell specification and
1083 migration in the simple chordate *Ciona intestinalis*. *Development* **132**, 4811-4818.
- 1084 Delsuc, F., Brinkmann, H., Chourrout, D., Philippe, H., 2006. Tunicates and not
1085 cephalochordates are the closest living relatives of vertebrates. *Nature* **439**, 965-968.
- 1086 Diogo, R., Kelly, R.G., Christiaen, L., Levine, M., Ziermann, J.M., Molnar, J.L.,
1087 Noden, D.M., Tzahor, E., 2015. A new heart for a new head in vertebrate
1088 cardiopharyngeal evolution. *Nature* **520**, 466-473.
- 1089 Dumollard, R., Minc, N., Salez, G., Aicha, S.B., Bekkouche, F., Hebras, C.,
1090 Besnardreau, L., McDougall, A., 2017. The invariant cleavage pattern displayed by
1091 ascidian embryos depends on spindle positioning along the cell's longest axis in the
1092 apical plane and relies on asynchronous cell divisions. *eLife* **6**.
- 1093 Farley, E.K., Olson, K.M., Zhang, W., Brandt, A.J., Rokhsar, D.S., Levine, M.S., 2015.
1094 Suboptimization of developmental enhancers. *Science* **350**, 325-328.
- 1095 Farley, E.K., Olson, K.M., Zhang, W., Rokhsar, D.S., Levine, M.S., 2016. Syntax
1096 compensates for poor binding sites to encode tissue specificity of developmental
1097 enhancers. *Proceedings of the National Academy of Sciences of the United States of
1098 America* **113**, 6508-6513.
- 1099 Gainous, T.B., Wagner, E., Levine, M., 2015. Diverse ETS transcription factors
1100 mediate FGF signaling in the *Ciona* anterior neural plate. *Developmental biology* **399**,
1101 218-225.
- 1102 Gandhi, S., Haeussler, M., Razy-Krajka, F., Christiaen, L., Stolfi, A., 2017. Evaluation
1103 and rational design of guide RNAs for efficient CRISPR/Cas9-mediated mutagenesis in
1104 *Ciona*. *Developmental biology* **425**, 8-20.
- 1105 George, V., Colombo, S., Targoff, K.L., 2015. An early requirement for nkx2.5 ensures
1106 the first and second heart field ventricular identity and cardiac function into adulthood.
1107 *Developmental biology* **400**, 10-22.
- 1108 Gopalakrishnan, S., Comai, G., Sambasivan, R., Francou, A., Kelly, R.G., Tajbakhsh,
1109 S., 2015. A Cranial Mesoderm Origin for Esophagus Striated Muscles. *Developmental
1110 cell* **34**, 694-704.
- 1111 Gotoh, N., Laks, S., Nakashima, M., Lax, I., Schlessinger, J., 2004. FRS2 family
1112 docking proteins with overlapping roles in activation of MAP kinase have distinct
1113 spatial-temporal patterns of expression of their transcripts. *FEBS letters* **564**, 14-18.

- 1114 Gueroult-Bellone, M., Nitta, K.R., Kari, W., Jacox, E., Beule Dauzat, R., Vincentelli,
1115 R., Diarra, C., Rothbacher, U., Dantec, C., Cambillau, C., Piette, J., Lemaire, P., 2017.
1116 Spacer sequences separating transcription factor binding motifs set enhancer quality and
1117 strength. *bioRxiv*.
- 1118 Hasson, P., Egoz, N., Winkler, C., Volohonsky, G., Jia, S., Dinur, T., Volk, T., Courey,
1119 A.J., Paroush, Z., 2005. EGFR signaling attenuates Groucho-dependent repression to
1120 antagonize Notch transcriptional output. *Nature genetics* 37, 101-105.
- 1121 Haupaix, N., Abitua, P.B., Sirour, C., Yasuo, H., Levine, M., Hudson, C., 2014. Ephrin-
1122 mediated restriction of ERK1/2 activity delimits the number of pigment cells in the
1123 Ciona CNS. *Developmental biology* 394, 170-180.
- 1124 Hotta, K., Mitsuhashara, K., Takahashi, H., Inaba, K., Oka, K., Gojobori, T., Ikeo, K.,
1125 2007. A web-based interactive developmental table for the ascidian *Ciona intestinalis*,
1126 including 3D real-image embryo reconstructions: I. From fertilized egg to hatching larva.
1127 *Developmental dynamics : an official publication of the American Association of*
1128 *Anatomists* 236, 1790-1805.
- 1129 Hu, T., Yamagishi, H., Maeda, J., McAnally, J., Yamagishi, C., Srivastava, D., 2004.
1130 *Tbx1* regulates fibroblast growth factors in the anterior heart field through a reinforcing
1131 autoregulatory loop involving forkhead transcription factors. *Development* 131, 5491-
1132 5502.
- 1133 Hudson, C., Darras, S., Caillol, D., Yasuo, H., Lemaire, P., 2003. A conserved role for
1134 the MEK signalling pathway in neural tissue specification and posteriorisation in the
1135 invertebrate chordate, the ascidian *Ciona intestinalis*. *Development* 130, 147-159.
- 1136 Hutson, M.R., Zeng, X.L., Kim, A.J., Antoon, E., Harward, S., Kirby, M.L., 2010.
1137 Arterial pole progenitors interpret opposing FGF/BMP signals to proliferate or
1138 differentiate. *Development* 137, 3001-3011.
- 1139 Ilagan, R., Abu-Issa, R., Brown, D., Yang, Y.P., Jiao, K., Schwartz, R.J., Klingensmith,
1140 J., Meyers, E.N., 2006. *Fgf8* is required for anterior heart field development.
1141 *Development* 133, 2435-2445.
- 1142 Imai, K.S., Levine, M., Satoh, N., Satou, Y., 2006. Regulatory blueprint for a chordate
1143 embryo. *Science* 312, 1183-1187.
- 1144 Imai, K.S., Satoh, N., Satou, Y., 2002. Early embryonic expression of FGF4/6/9 gene
1145 and its role in the induction of mesenchyme and notochord in *Ciona savignyi* embryos.
1146 *Development* 129, 1729-1738.
- 1147 Jeffery, W.R., Chiba, T., Krajka, F.R., Deyts, C., Satoh, N., Joly, J.S., 2008. Trunk
1148 lateral cells are neural crest-like cells in the ascidian *Ciona intestinalis*: insights into the
1149 ancestry and evolution of the neural crest. *Developmental biology* 324, 152-160.
- 1150 Jerome, L.A., Papaioannou, V.E., 2001. DiGeorge syndrome phenotype in mice
1151 mutant for the T-box gene, *Tbx1*. *Nature genetics* 27, 286-291.

- 1152 Kaplan, N., Razy-Krajka, F., Christiaen, L., 2015. Regulation and evolution of
1153 cardiopharyngeal cell identity and behavior: insights from simple chordates. Current
1154 opinion in genetics & development 32, 119-128.
- 1155 Kattman, S.J., Witty, A.D., Gagliardi, M., Dubois, N.C., Niapour, M., Hotta, A., Ellis,
1156 J., Keller, G., 2011. Stage-specific optimization of activin/nodal and BMP signaling
1157 promotes cardiac differentiation of mouse and human pluripotent stem cell lines. Cell
1158 stem cell 8, 228-240.
- 1159 Keduka, E., Kaiho, A., Hamada, M., Watanabe-Takano, H., Takano, K., Ogasawara,
1160 M., Satou, Y., Satoh, N., Endo, T., 2009. M-Ras evolved independently of R-Ras and its
1161 neural function is conserved between mammalian and ascidian, which lacks classical
1162 Ras. Gene 429, 49-58.
- 1163 Kelly, R.G., Jerome-Majewska, L.A., Papaioannou, V.E., 2004. The del22q11.2
1164 candidate gene Tbx1 regulates branchiomeric myogenesis. Human molecular genetics 13,
1165 2829-2840.
- 1166 Kelly, R.G., Papaioannou, V.E., 2007. Visualization of outflow tract development in
1167 the absence of Tbx1 using an Fgf10 enhancer trap transgene. Developmental dynamics :
1168 an official publication of the American Association of Anatomists 236, 821-828.
- 1169 Khoueiry, P., Rothbacher, U., Ohtsuka, Y., Daian, F., Frangulian, E., Roure, A.,
1170 Dubchak, I., Lemaire, P., 2010. A cis-regulatory signature in ascidians and flies,
1171 independent of transcription factor binding sites. Current biology : CB 20, 792-802.
- 1172 Kuwajima, M., Kumano, G., Nishida, H., 2014. Regulation of the number of cell
1173 division rounds by tissue-specific transcription factors and Cdk inhibitor during ascidian
1174 embryogenesis. PloS one 9, e90188.
- 1175 Lemmon, M.A., Schlessinger, J., 2010. Cell signaling by receptor tyrosine kinases. Cell
1176 141, 1117-1134.
- 1177 Lescroart, F., Chabab, S., Lin, X., Rulands, S., Paulissen, C., Rodolosse, A., Auer, H.,
1178 Achouri, Y., Dubois, C., Bondue, A., Simons, B.D., Blanpain, C., 2014. Early lineage
1179 restriction in temporally distinct populations of Mesp1 progenitors during mammalian
1180 heart development. Nature cell biology 16, 829-840.
- 1181 Lescroart, F., Hamou, W., Francou, A., Theveniau-Ruissy, M., Kelly, R.G.,
1182 Buckingham, M., 2015. Clonal analysis reveals a common origin between nonsomite-
1183 derived neck muscles and heart myocardium. Proceedings of the National Academy of
1184 Sciences of the United States of America 112, 1446-1451.
- 1185 Lescroart, F., Kelly, R.G., Le Garrec, J.F., Nicolas, J.F., Meilhac, S.M., Buckingham,
1186 M., 2010. Clonal analysis reveals common lineage relationships between head muscles
1187 and second heart field derivatives in the mouse embryo. Development 137, 3269-3279.
- 1188 Lescroart, F., Mohun, T., Meilhac, S.M., Bennett, M., Buckingham, M., 2012. Lineage
1189 tree for the venous pole of the heart: clonal analysis clarifies controversial genealogy
1190 based on genetic tracing. Circulation research 111, 1313-1322.

- 1191 Mandal, A., Holowiecki, A., Song, Y.C., Waxman, J.S., 2017. Wnt signaling balances
1192 specification of the cardiac and pharyngeal muscle fields. *Mechanisms of Development*
1193 143, 32-41.
- 1194 Mansour, S.J., Resing, K.A., Candi, J.M., Hermann, A.S., Gloor, J.W., Herskind, K.R.,
1195 Wartmann, M., Davis, R.J., Ahn, N.G., 1994. Mitogen-activated protein (MAP) kinase
1196 phosphorylation of MAP kinase kinase: determination of phosphorylation sites by mass
1197 spectrometry and site-directed mutagenesis. *Journal of biochemistry* 116, 304-314.
- 1198 Marques, S.R., Lee, Y., Poss, K.D., Yelon, D., 2008. Reiterative roles for FGF signaling
1199 in the establishment of size and proportion of the zebrafish heart. *Developmental biology*
1200 321, 397-406.
- 1201 Mazzoni, E.O., Mahony, S., Iacovino, M., Morrison, C.A., Mountoufaris, G., Closser,
1202 M., Whyte, W.A., Young, R.A., Kyba, M., Gifford, D.K., Wichterle, H., 2011. Embryonic
1203 stem cell-based mapping of developmental transcriptional programs. *Nature methods* 8,
1204 1056-1058.
- 1205 Merscher, S., Funke, B., Epstein, J.A., Heyer, J., Puech, A., Lu, M.M., Xavier, R.J.,
1206 Demay, M.B., Russell, R.G., Factor, S., Tokooya, K., Jore, B.S., Lopez, M., Pandita, R.K.,
1207 Lia, M., Carrion, D., Xu, H., Schorle, H., Kobler, J.B., Scambler, P., Wynshaw-Boris, A.,
1208 Skoultschi, A.I., Morrow, B.E., Kucherlapati, R., 2001. TBX1 is responsible for
1209 cardiovascular defects in velo-cardio-facial/DiGeorge syndrome. *Cell* 104, 619-629.
- 1210 Michailovici, I., Eigler, T., Tzahor, E., 2015. Craniofacial Muscle Development.
1211 *Current topics in developmental biology* 115, 3-30.
- 1212 Michailovici, I., Harrington, H.A., Azogui, H.H., Yahalom-Ronen, Y., Plotnikov, A.,
1213 Ching, S., Stumpf, M.P., Klein, O.D., Seger, R., Tzahor, E., 2014. Nuclear to cytoplasmic
1214 shuttling of ERK promotes differentiation of muscle stem/progenitor cells. *Development*
1215 141, 2611-2620.
- 1216 Mosimann, C., Panakova, D., Werdich, A.A., Musso, G., Burger, A., Lawson, K.L.,
1217 Carr, L.A., Nevis, K.R., Sabeh, M.K., Zhou, Y., Davidson, A.J., DiBiase, A., Burns, C.E.,
1218 Burns, C.G., MacRae, C.A., Zon, L.I., 2015. Chamber identity programs drive early
1219 functional partitioning of the heart. *Nature communications* 6, 8146.
- 1220 Nathan, E., Monovich, A., Tirosh-Finkel, L., Harrelson, Z., Rousso, T., Rinon, A.,
1221 Harel, I., Evans, S.M., Tzahor, E., 2008. The contribution of Islet1-expressing splanchnic
1222 mesoderm cells to distinct branchiomeric muscles reveals significant heterogeneity in
1223 head muscle development. *Development* 135, 647-657.
- 1224 Nevis, K., Obregon, P., Walsh, C., Guner-Ataman, B., Burns, C.G., Burns, C.E., 2013.
1225 Tbx1 is required for second heart field proliferation in zebrafish. *Developmental
1226 dynamics : an official publication of the American Association of Anatomists* 242, 550-
1227 559.
- 1228 Norton, J., Cooley, J., Islam, A.F., Cota, C.D., Davidson, B., 2013. Matrix adhesion
1229 polarizes heart progenitor induction in the invertebrate chordate *Ciona intestinalis*.
1230 *Development* 140, 1301-1311.

- 1231 Park, E.J., Ogden, L.A., Talbot, A., Evans, S., Cai, C.L., Black, B.L., Frank, D.U., Moon,
1232 A.M., 2006. Required, tissue-specific roles for Fgf8 in outflow tract formation and
1233 remodeling. *Development* 133, 2419-2433.
- 1234 Park, E.J., Watanabe, Y., Smyth, G., Miyagawa-Tomita, S., Meyers, E., Klingensmith,
1235 J., Camenisch, T., Buckingham, M., Moon, A.M., 2008. An FGF autocrine loop initiated
1236 in second heart field mesoderm regulates morphogenesis at the arterial pole of the heart.
1237 *Development* 135, 3599-3610.
- 1238 Patterson, K.I., Brummer, T., O'Brien, P.M., Daly, R.J., 2009. Dual-specificity
1239 phosphatases: critical regulators with diverse cellular targets. *The Biochemical journal*
1240 418, 475-489.
- 1241 Pauklin, S., Madrigal, P., Bertero, A., Vallier, L., 2016. Initiation of stem cell
1242 differentiation involves cell cycle-dependent regulation of developmental genes by Cyclin
1243 D. *Genes & development* 30, 421-433.
- 1244 Pauklin, S., Vallier, L., 2013. The cell-cycle state of stem cells determines cell fate
1245 propensity. *Cell* 155, 135-147.
- 1246 Peljto, M., Wichterle, H., 2011. Programming embryonic stem cells to neuronal
1247 subtypes. *Current opinion in neurobiology* 21, 43-51.
- 1248 Pennati, R., Ficetola, G.F., Brunetti, R., Caicci, F., Gasparini, F., Griggio, F., Sato, A.,
1249 Stach, T., Kaul-Strehlow, S., Gissi, C., Manni, L., 2015. Morphological Differences
1250 between Larvae of the *Ciona intestinalis* Species Complex: Hints for a Valid Taxonomic
1251 Definition of Distinct Species. *PloS one* 10, e0122879.
- 1252 Picco, V., Hudson, C., Yasuo, H., 2007. Ephrin-Eph signalling drives the asymmetric
1253 division of notochord/neural precursors in *Ciona* embryos. *Development* 134, 1491-1497.
- 1254 Prall, O.W., Menon, M.K., Solloway, M.J., Watanabe, Y., Zaffran, S., Bajolle, F., Biben,
1255 C., McBride, J.J., Robertson, B.R., Chaulet, H., Stennard, F.A., Wise, N., Schaft, D.,
1256 Wolstein, O., Furtado, M.B., Shiratori, H., Chien, K.R., Hamada, H., Black, B.L., Saga, Y.,
1257 Robertson, E.J., Buckingham, M.E., Harvey, R.P., 2007. An Nkx2-5/Bmp2/Smad1
1258 negative feedback loop controls heart progenitor specification and proliferation. *Cell* 128,
1259 947-959.
- 1260 Putnam, N.H., Butts, T., Ferrier, D.E., Furlong, R.F., Hellsten, U., Kawashima, T.,
1261 Robinson-Rechavi, M., Shoguchi, E., Terry, A., Yu, J.K., Benito-Gutierrez, E.L., Dubchak,
1262 I., Garcia-Fernandez, J., Gibson-Brown, J.J., Grigoriev, I.V., Horton, A.C., de Jong, P.J.,
1263 Jurka, J., Kapitonov, V.V., Kohara, Y., Kuroki, Y., Lindquist, E., Lucas, S., Osoegawa, K.,
1264 Pennacchio, L.A., Salamov, A.A., Satou, Y., Sauka-Spengler, T., Schmutz, J., Shin, I.T.,
1265 Toyoda, A., Bronner-Fraser, M., Fujiyama, A., Holland, L.Z., Holland, P.W., Satoh, N.,
1266 Rokhsar, D.S., 2008. The amphioxus genome and the evolution of the chordate
1267 karyotype. *Nature* 453, 1064-1071.
- 1268 Racioppi, C., Kamal, A.K., Razy-Krajka, F., Gambardella, G., Zanetti, L., di Bernardo,
1269 D., Sanges, R., Christiaen, L.A., Ristoratore, F., 2014. Fibroblast growth factor signalling
1270 controls nervous system patterning and pigment cell formation in *Ciona intestinalis*.
1271 *Nature communications* 5, 4830.

- 1272 Razy-Krajka, F., Lam, K., Wang, W., Stolfi, A., Joly, M., Bonneau, R., Christiaen, L.,
1273 2014. Collier/OLF/EBF-Dependent Transcriptional Dynamics Control Pharyngeal
1274 Muscle Specification from Primed Cardiopharyngeal Progenitors. *Developmental cell* 29,
1275 263-276.
- 1276 Reifers, F., Walsh, E.C., Leger, S., Stainier, D.Y., Brand, M., 2000. Induction and
1277 differentiation of the zebrafish heart requires fibroblast growth factor 8
1278 (fgf8/acerebellar). *Development* 127, 225-235.
- 1279 Satou, Y., Imai, K.S., Satoh, N., 2004. The ascidian Mesp gene specifies heart
1280 precursor cells. *Development* 131, 2533-2541.
- 1281 Shi, W., Levine, M., 2008. Ephrin signaling establishes asymmetric cell fates in an
1282 endomesoderm lineage of the Ciona embryo. *Development* 135, 931-940.
- 1283 Shi, W., Peyrot, S.M., Munro, E., Levine, M., 2009. FGF3 in the floor plate directs
1284 notochord convergent extension in the Ciona tadpole. *Development* 136, 23-28.
- 1285 Soufi, A., Dalton, S., 2016. Cycling through developmental decisions: how cell cycle
1286 dynamics control pluripotency, differentiation and reprogramming. *Development* 143,
1287 4301-4311.
- 1288 Stolfi, A., Gainous, T.B., Young, J.J., Mori, A., Levine, M., Christiaen, L., 2010. Early
1289 chordate origins of the vertebrate second heart field. *Science* 329, 565-568.
- 1290 Stolfi, A., Gandhi, S., Salek, F., Christiaen, L., 2014a. Tissue-specific genome editing
1291 in Ciona embryos by CRISPR/Cas9. *Development* 141, 4115-4120.
- 1292 Stolfi, A., Lowe, E.K., Racioppi, C., Ristoratore, F., Brown, C.T., Swalla, B.J.,
1293 Christiaen, L., 2014b. Divergent mechanisms regulate conserved cardiopharyngeal
1294 development and gene expression in distantly related ascidians. *eLife* 3, e03728.
- 1295 Stolfi, A., Sasakura, Y., Satou, Y., Christiaen, L., Dantec, C., Endo, T., Naville, M.,
1296 Nishida, H., Swalla, B., Volff, J.-N., Voskoboynik, A., Dauga, D., Lemaire, P., 2014c.
1297 Guidelines for the Nomenclature of Genetic Elements in Tunicate Genomes. *Genesis*
1298 under review.
- 1299 Stolfi, A., Wagner, E., Taliaferro, J.M., Chou, S., Levine, M., 2011. Neural tube
1300 patterning by Ephrin, FGF and Notch signaling relays. *Development* 138, 5429-5439.
- 1301 Tirosh-Finkel, L., Elhanany, H., Rinon, A., Tzahor, E., 2006. Mesoderm progenitor
1302 cells of common origin contribute to the head musculature and the cardiac outflow tract.
1303 *Development* 133, 1943-1953.
- 1304 Tirosh-Finkel, L., Zeisel, A., Brodt-Ivenshitz, M., Shamai, A., Yao, Z., Seger, R.,
1305 Domany, E., Tzahor, E., 2010. BMP-mediated inhibition of FGF signaling promotes
1306 cardiomyocyte differentiation of anterior heart field progenitors. *Development* 137,
1307 2989-3000.
- 1308 Tolkin, T., Christiaen, L., 2016. Rewiring of an ancestral Tbx1/10-Ebf-Mrf network for
1309 pharyngeal muscle specification in distinct embryonic lineages. *Development* in press.

- 1310 Tzahor, E., 2009. Heart and craniofacial muscle development: a new developmental
1311 theme of distinct myogenic fields. *Developmental biology* 327, 273-279.
- 1312 Tzahor, E., Evans, S.M., 2011. Pharyngeal mesoderm development during
1313 embryogenesis: implications for both heart and head myogenesis. *Cardiovascular*
1314 research 91, 196-202.
- 1315 Tzahor, E., Kempf, H., Mootoosamy, R.C., Poon, A.C., Abzhanov, A., Tabin, C.J.,
1316 Dietrich, S., Lassar, A.B., 2003. Antagonists of Wnt and BMP signaling promote the
1317 formation of vertebrate head muscle. *Genes & development* 17, 3087-3099.
- 1318 Tzahor, E., Lassar, A.B., 2001. Wnt signals from the neural tube block ectopic
1319 cardiogenesis. *Genes & development* 15, 255-260.
- 1320 van Wijk, B., van den Berg, G., Abu-Issa, R., Barnett, P., van der Velden, S., Schmidt,
1321 M., Ruijter, J.M., Kirby, M.L., Moorman, A.F., van den Hoff, M.J., 2009. Epicardium
1322 and myocardium separate from a common precursor pool by crosstalk between bone
1323 morphogenetic protein- and fibroblast growth factor-signaling pathways. *Circulation*
1324 research 105, 431-441.
- 1325 Vitelli, F., Morishima, M., Taddei, I., Lindsay, E.A., Baldini, A., 2002a. Tbx1 mutation
1326 causes multiple cardiovascular defects and disrupts neural crest and cranial nerve
1327 migratory pathways. *Human molecular genetics* 11, 915-922.
- 1328 Vitelli, F., Taddei, I., Morishima, M., Meyers, E.N., Lindsay, E.A., Baldini, A., 2002b.
1329 A genetic link between Tbx1 and fibroblast growth factor signaling. *Development* 129,
1330 4605-4611.
- 1331 von Scheven, G., Alvares, L.E., Mootoosamy, R.C., Dietrich, S., 2006. Neural tube
1332 derived signals and Fgf8 act antagonistically to specify eye versus mandibular arch
1333 muscles. *Development* 133, 2731-2745.
- 1334 Wagner, E., Stolfi, A., Gi Choi, Y., Levine, M., 2014. Islet is a key determinant of
1335 ascidian palp morphogenesis. *Development* 141, 3084-3092.
- 1336 Wang, W., Razy-Krajka, F., Siu, E., Ketcham, A., Christiaen, L., 2013. NK4
1337 antagonizes Tbx1/10 to promote cardiac versus pharyngeal muscle fate in the ascidian
1338 second heart field. *PLoS biology* 11, e1001725.
- 1339 Wang, W., Xiang, S., Jullian, E., Kelly, R.G., Satija, R., Christiaen, L., 2017. A single
1340 cell transcriptional roadmap for cardiopharyngeal fate diversification. *BioRxiv*.
- 1341 Watanabe, Y., Miyagawa-Tomita, S., Vincent, S.D., Kelly, R.G., Moon, A.M.,
1342 Buckingham, M.E., 2010. Role of mesodermal FGF8 and FGF10 overlaps in the
1343 development of the arterial pole of the heart and pharyngeal arch arteries. *Circulation*
1344 research 106, 495-503.
- 1345 Watanabe, Y., Zaffran, S., Kuroiwa, A., Higuchi, H., Ogura, T., Harvey, R.P., Kelly,
1346 R.G., Buckingham, M., 2012. Fibroblast growth factor 10 gene regulation in the second
1347 heart field by Tbx1, Nkx2-5, and Islet1 reveals a genetic switch for down-regulation in the
1348 myocardium. *Proceedings of the National Academy of Sciences of the United States of*
1349 *America* 109, 18273-18280.

- 1350 Whittaker, J.R., 1973. Segregation during ascidian embryogenesis of egg cytoplasmic
1351 information for tissue-specific enzyme development. *Proceedings of the National
1352 Academy of Sciences of the United States of America* 70, 2096-2100.
- 1353 Witzel, H.R., Cheedipudi, S., Gao, R., Stainier, D.Y., Dobreva, G.D., 2017. *Isl2b*
1354 regulates anterior second heart field development in zebrafish. *Scientific reports* 7,
1355 41043.
- 1356 Woznica, A., Haeussler, M., Starobinska, E., Jemmett, J., Li, Y., Mount, D., Davidson,
1357 B., 2012. Initial deployment of the cardiogenic gene regulatory network in the basal
1358 chordate, *Ciona intestinalis*. *Developmental biology* 368, 127-139.
- 1359 Yagi, H., Furutani, Y., Hamada, H., Sasaki, T., Asakawa, S., Minoshima, S., Ichida, F.,
1360 Joo, K., Kimura, M., Imamura, S., Kamatani, N., Momma, K., Takao, A., Nakazawa, M.,
1361 Shimizu, N., Matsuoka, R., 2003. Role of TBX1 in human del22q11.2 syndrome. *Lancet*
1362 362, 1366-1373.
- 1363 Yasuo, H., Hudson, C., 2007. FGF8/17/18 functions together with FGF9/16/20 during
1364 formation of the notochord in *Ciona* embryos. *Developmental biology* 302, 92-103.
- 1365 Zaffran, S., Frasch, M., 2002. Early signals in cardiac development. *Circulation
1366 research* 91, 457-469.
- 1367 Zhang, Z., Huynh, T., Baldini, A., 2006. Mesodermal expression of *Tbx1* is necessary
1368 and sufficient for pharyngeal arch and cardiac outflow tract development. *Development*
1369 133, 3587-3595.
1370